Developments in the Built Environment 26 (2026) 100930

Contents lists available at ScienceDirect

Developments in the Built Environment

journal homepage: www.sciencedirect.com/journal/developments-in-the-built-environment

# From laboratory formulation to in situ evaluation: PCM-enhanced lime-pozzolan-cement mortars for thermal retrofit of heritage architecture

Loucas Kyriakou [a], Andrea Rubio-Aguinaga [a], Mohammad Hossein Nofalah [a], Laura Maria Piarulli Paz [b], Álvaro García Molino [c], Liberato Ferrara [d], Ioannis Karatasios [e], Eirini Tziviloglou [e], José María Fernández [a], Íñigo Navarro-Blasco [a], José Ignacio Álvarez [a,*]

[a] Materials and Cultural Heritage (MATCH) Research Group, Department of Chemistry, School of Sciences, University of Navarra, C/ Irunlarrea 1, Navarra, Pamplona, 31008, Spain
[b] Fundación Agustín de Betancourt, ETSI Caminos Canales y Puertos, Calle del Profesor Aranguren 3, Madrid, 28040, Spain
[c] Acciona Construction S.A., Calle Valportillo Segunda 8, Madrid, 28108, Spain
[d] Department of Civil and Environmental Engineering, Politecnico di Milano, Milan, Italy
[e] Institute of Nanoscience and Nanotechnology, N.C.S.R. "Demokritos", Patr. Gregoriou E & 27 Neapoleos Str., Agia Paraskevi, 15341, Greece

ARTICLE INFO

*Keywords:*
Phase change materials (PCM)
Lime-cement mortars
Heritage buildings
Thermal retrofitting
Thermal inertia
Durability
Field monitoring

ABSTRACT

The energy retrofitting of heritage buildings is constrained by strict requirements on material compatibility, reversibility, and minimal intervention, limiting the use of conventional insulation systems. In this context, lime-based rendering mortars incorporating phase change materials (PCMs) offer a promising solution for enhancing thermal performance while respecting conservation principles. This study investigates the suitability of PCM-enhanced ternary lime-pozzolan-cement mortars through a combined laboratory and field-scale experimental approach, with particular emphasis on real-scale validation under outdoor conditions.

Mortars incorporating microencapsulated PCMs were characterized in terms of microstructure, hygric and mechanical properties, thermal conductivity, and latent heat storage, alongside durability assessment under freeze-thaw and salt crystallization cycles. Thermal performance was evaluated using hot-box testing and monitored full-scale mock-ups exposed to real climatic conditions.

The results show that PCM incorporation significantly reduces thermal conductivity (from ca. 0.63 to 0.30 W $m^{-1}\cdot K^{-1}$) while providing latent heat storage up to 2.7 J $g^{-1}$. Durability performance was maintained or improved compared to reference mortars. Both laboratory and field-scale results demonstrate the ability of PCM-enhanced mortars to attenuate temperature fluctuations, leading to smoother internal temperature profiles and reduced thermal peaks under real environmental conditions.

Overall, the findings confirm that PCM-enhanced ternary lime-based mortars can provide passive thermal buffering while maintaining compatibility with heritage substrates, supporting their application in conservation-oriented energy retrofitting strategies.

## 1. Introduction

The building sector is among the largest contributors to global energy consumption and greenhouse-gas emissions, primarily due to heating and cooling demands associated with existing buildings (Pajek et al., 2022; Asadi et al., 2012). In Europe, a substantial proportion of the building stock predates the introduction of modern energy-efficiency regulations and is characterized by limited thermal performance (Baccega and Bottarelli, 2025; Tripathi and Shukla, 2024). The refurbishment of this stock is therefore a key strategy for reducing operational energy demand and improving indoor comfort. However, when buildings are protected for their historical, architectural, or cultural

* Corresponding author.
*E-mail addresses:* lkyriakou@unav.es (L. Kyriakou), arubioa@unav.es (A. Rubio-Aguinaga), mnofalah@unav.es (M.H. Nofalah), lpiarulli@fundacionabetancourt.org (L.M. Piarulli Paz), alvaro.garcia.molino@acciona.com (Á. García Molino), liberato.ferrara@polimi.it (L. Ferrara), i.karatasios@inn.demokritos.gr (I. Karatasios), e.tziviloglou@inn.demokritos.gr (E. Tziviloglou), jmfdez@unav.es (J.M. Fernández), inavarro@unav.es (Í. Navarro-Blasco), jalvarez@unav.es (J.I. Álvarez).

https://doi.org/10.1016/j.dibe.2026.100930
Received 2 March 2026; Received in revised form 15 April 2026; Accepted 21 April 2026
Available online 27 April 2026

value, energy retrofitting is subject to strict regulatory and conservation constraints that significantly restrict the range of admissible interventions (Milone et al., 2015; Martín-Garín et al., 2021). Conventional retrofit solutions, including, e.g., external thermal insulation composite systems or invasive internal linings, are often incompatible with protected façades, architectural detailing, or original materials, and may introduce hygrothermal risks if improperly applied (Odgaard et al., 2018; Blumberga et al., 2023). Consequently, there is a clear need for retrofit approaches that enhance thermal performance while respecting conservation principles and material compatibility.

Within this framework, lime-based mortars and plasters remain central to conservation practice due to their chemical and physical affinity with traditional masonry substrates, relatively low stiffness, and high vapour permeability, which facilitate moisture transport and enhance the overall breathability of historic walls (Groot et al., 2022; Sala et al., 2016). These characteristics make lime mortars particularly suitable as repair and rendering materials for heritage buildings, where incompatibility between original substrates and modern cementitious products has historically led to premature damage (Groot et al., 2022; Barbosa et al., 2023; Kumar and Kumar, 2022; Santos et al., 2023). Nevertheless, the intrinsic thermal conductivity of conventional lime mortars limits their contribution to thermal upgrading when used alone and within thicknesses acceptable for conservation contexts (Martín-Garín et al., 2021). As a result, recent research has increasingly focused on functionalized lime-based mortars designed to improve thermal performance while retaining compatibility with historic envelopes (Rubio-Aguinaga et al., 2025a, 2025b).

Among functionalization strategies, the incorporation of phase change materials (PCMs) has received considerable attention as a means of introducing latent heat thermal energy storage into building envelope components (Akeiber et al., 2016; Frigione et al., 2019). PCMs absorb and release substantial amounts of energy during phase transitions occurring within a defined temperature range, thereby increasing effective thermal inertia and moderating temperature fluctuations under cyclic thermal loadings (Ferencz et al., 2025; Tian et al., 2025). When integrated into mortars or plasters, PCMs can reduce peak heat fluxes through wall assemblies and delay heat transfer, provided that the phase change temperature aligns with the operative temperature range and that complete charge–discharge cycles occur (Sinka et al., 2019; Illampas et al., 2021). This approach is particularly attractive for heritage applications, where limited thickness and preservation of surface appearance restrict the use of conventional insulation systems (Ventolà et al., 2013; Posani et al., 2021).

To enable the incorporation of PCMs into cementitious matrices, microencapsulation is widely employed to prevent leakage during melting and to improve heat transfer and maintain structural integrity during phase transitions within the binder system (Asadi et al., 2022; Liu et al., 2019). The PCM is enclosed within a protective shell, which ensures its retention in liquid state and avoids direct interaction with the surrounding matrix. Numerous studies have demonstrated that microencapsulated PCMs (mPCMs) can be successfully integrated into mortars and plasters, leading to measurable increases in heat storage capacity and reductions in thermal conductivity when appropriately formulated (Theodoridou et al., 2016; Li et al., 2024). In lime-based matrices, laboratory investigations have shown that mPCMs incorporation modifies thermophysical properties and enhances thermal buffering without fundamentally altering the nature of the binder when moderate PCM dosages are employed (Sarcinella et al., 2020). More recent work on hydrated lime rendering mortars has further linked microstructural observations, such as pore size distribution and capsule-matrix interaction, to thermal performance outcomes (Rubio-Aguinaga et al., 2024a).

At the same time, PCM incorporation, besides requiring tailored adjustment to the rheology of the fresh mixtures to guarantee their ease of application through, e.g., conventional plastering or casting technologies, is known to influence mechanical behaviour and durability, and the literature consistently highlights the importance of dosage control (Frahat et al., 2023; Zheng et al., 2025). The introduction of microcapsules in the matrix may lead to reduced compressive and flexural strength, increased porosity, or altered fracture behaviour, particularly at higher PCM contents (Frigione et al., 2019; Coppola et al., 2016). Experimental and monitoring studies have reported that excessive PCM dosages can result in surface deterioration or cohesion loss, likely associated with volumetric changes during phase transitions or insufficient binder continuity (Baccega and Bottarelli, 2025; Drissi et al., 2019). These findings underline the need for optimized mix designs that balance thermal functionality with mechanical integrity and long-term performance (Rubio-Aguinaga et al., 2024a).

In addition to lime-based systems, extensive research has been conducted on the incorporation of PCMs into cementitious materials, including mortars and concretes, to enhance thermal energy storage capacity. Previous studies have consistently shown that PCM incorporation leads to reduced thermal conductivity and improved thermal inertia, enabling attenuation of temperature fluctuations and delayed heat transfer under cyclic thermal conditions. For instance, Shi et al. reported that increasing PCM content in lightweight aggregate mortars significantly decreases thermal conductivity and enhances thermal regulation capacity, although this is often accompanied by increased porosity and reduced mechanical strength due to the presence of microcapsules within the matrix (Shi et al., 2020). Similarly, studies on nano-PCM-enhanced building components have demonstrated improved thermal buffering performance through both experimental and numerical approaches (Biswas et al., 2014). These findings highlight the inherent trade-off between thermal functionality and mechanical performance, emphasizing the need for optimized formulations tailored to the specific binder system and application requirements.

Durability under environmental loading is a critical requirement for any mortar intended for heritage or exposed envelope applications. Freeze-thaw cycling and salt crystallization are among the most aggressive degradation mechanisms affecting porous cementitious materials, particularly in moisture-rich historic masonry (Rodríguez et al., 2020; Pavlíková et al., 2021). Recent studies have suggested that PCMs may influence durability both positively and negatively, depending on formulation. On the one hand, thermal buffering associated with latent heat storage may reduce the frequency and intensity of freeze-thaw events within the pore network (Šavija, 2018; Yeon and Kim, 2018). On the other hand, excessive PCM content or poor capsule integration may weaken the matrix and increase susceptibility to damage (Rodríguez et al., 2020). For lime-based systems specifically, emerging evidence indicates that carefully designed PCM-lime mortars can maintain or even improve resistance to freeze-thaw and salt crystallization compared to reference mortars, although available datasets remain limited (Rubio-Aguinaga et al., 2025b; Pavlíková et al., 2021). As such, durability assessment remains a key knowledge gap in the development of PCM-enhanced mortars for conservation and retrofit purposes.

Another critical aspect concerns the transferability of laboratory performance to field conditions. Hygrothermal studies of historic walls have repeatedly demonstrated that real-world behaviour depends strongly on boundary conditions, substrate heterogeneity, workmanship, and detailing at interfaces and junctions (Odgaard et al., 2018; Blumberga et al., 2023). For PCM-based systems, laboratory measurements of latent heat, conductivity, or heat capacity are necessary but insufficient predictors of in-situ performance, since PCM activation depends on actual temperature histories and heat-flux dynamics (Baccega and Bottarelli, 2025; Sinka et al., 2019). Consequently, monitored mock-ups and field-scale experiments are increasingly recognized as essential tools for validating PCM functionality under realistic climatic exposure (Baccega and Bottarelli, 2022, 2025).

In this study, additional field-relevant evidence is provided through sensor-based monitoring of full-scale mock-ups, where the lime-based mortar formulation developed by the authors and incorporating

microencapsulated PCM was applied to a test wall and directly compared with an otherwise identical reference wall without PCM. Temperature measurements collected within the mock-ups allow assessment of the PCM contribution under comparable outdoor boundary conditions and support the interpretation of laboratory findings.

Finally, it is important to frame material compatibility within the evolving definition of cultural heritage, which today encompasses not only traditional masonry structures but also a growing body of 20th-century reinforced-concrete architecture (Marcos et al., 2016; Miranda et al., 2022; Redondo et al., 2021). Conservation of historic concrete often requires repair mortars that combine cementitious compatibility, durability, and visual integration, challenging the traditional exclusion of cement-based binders from heritage contexts (Redondo et al., 2021). In this regard, the use of limited amounts of white cement (at contents below 25 %) within predominantly lime-based mortars can be interpreted as a pragmatic strategy aimed at addressing the needs of both traditional masonry and modern concrete heritage, provided that overall compatibility, vapour permeability, and durability are preserved (Andrejkovičová et al., 2022; Silva et al., 2025).

Within this context, the present study was developed in the framework of the Horizon Europe SINCERE project (GA101123293), which focuses on the design, assessment, and demonstration of sustainable material solutions for the energy-efficient retrofitting of existing and heritage buildings. The project promotes an integrated methodology that links laboratory-scale material development with pilot-scale validation under real environmental conditions. The experimental programme presented herein reflects this approach by combining detailed material characterization with monitored field application, allowing the performance of PCM-enhanced lime-cement-based mortars to be evaluated beyond controlled laboratory conditions.

The aim of this study is to evaluate the suitability of ternary (lime-pozzolan-cement) mortars incorporating microencapsulated phase change materials for the thermal retrofitting of buildings, with particular emphasis on challenges associated with field application. The work provides: (i) laboratory characterization of thermophysical, microstructural, and mechanical properties; (ii) durability assessment of the mortars under freeze-thaw and salt crystallization cycles; and (iii) validation through monitored mock-up testing comparing PCM-modified and reference mortars under real climatic exposure. The novelty of the study lies in its integrated approach, combining thermal functionality, durability performance, and field-scale validation within a material framework explicitly positioned for both traditional masonry heritage and modern concrete heritage. By addressing these aspects simultaneously, the paper contributes evidence necessary for the informed and conservation-aligned deployment of PCM-enhanced lime-based mortars in practice.

## 2. Materials and methods

### 2.1. Materials

Mortars were formulated using hydrated calcitic lime (CL 90-S) supplied by Cal Industrial S.A. (Navarra, Spain). It complies with the requirements of EN 459-1 (Building Lime, 2011) for CL 90-S limes and exhibits an average particle size of approximately 10 μm, with less than 10 % of particles exceeding 50 μm in diameter. The chemical composition of the lime was characterized by X-ray fluorescence (XRF) analysis using a Bruker S2 PUMA spectrometer (Bruker Scientific Instruments, Billerica, MA, USA) equipped with a silver anode X-ray tube. Measurements were conducted under a helium atmosphere with a 4 μm polypropylene filter, and quantitative data were processed using Spectra Results Manager software (Bruker AXS Spectra Elements v2.3). The XRF results indicated a CaO content of 96.54 wt%, with minor constituents including $SO_3$ (1.29 wt%) and $SiO_2$ (0.82 wt%).

A natural pozzolana supplied by TITAN Cement Group (Greece) was used as a supplementary cementitious component in the binder system. The material is of volcanic origin and is characterized by a siliceous-aluminous composition, typical of natural pozzolanic materials employed in lime-based and blended binders. X-ray fluorescence (XRF) analysis indicates that the pozzolana is rich in reactive oxides, with $SiO_2$ (71.07 wt%) and $Al_2O_3$ (14.55 wt%) as the dominant constituents, accompanied by moderate contents of $Fe_2O_3$ (1.56 wt%), CaO (3.77 wt %), MgO (2.69 wt%), and $K_2O$ (4.39 wt%). Minor amounts of $TiO_2$ (1.24 wt%) and trace oxides were also detected, while $SO_3$ and $Cl^-$ contents were negligible. The high combined content of silica and alumina confirms the pozzolanic nature of the material and its suitability for use in lime-bearing composite binders, where it can contribute to secondary hydrate formation through pozzolanic reactions with calcium hydroxide, enhancing long-term mechanical performance and durability.

A white Portland cement with limestone addition (type BL II/B-L 42.5 N) supplied by Cementos Portland Valderrivas S.A. (Madrid, Spain) was used as a minor binder component in selected mortar formulations. The cement complies with the requirements of EN 197-1 (Cement, 2011) for common cements and is characterized by a fine particle size distribution, with an average particle size of approximately 10 μm. According to the manufacturer's specifications, the cement composition is characterized by a high calcium oxide (CaO) content of 96.54 wt% (Rubio-Aguinaga et al., 2024b), reflecting its high purity and suitability for applications where colour stability, controlled reactivity, and compatibility with mineral binders are required.

A standardized siliceous sand complying with EN 196-1 specifications (Methods of Testing, 2018) was used as aggregate for mortar preparation. The sand corresponds to CEN standard sand and presents a well-defined and reproducible particle size distribution, ensuring consistency across all mixtures. The sand exhibits a controlled and well-graded particle size distribution predominantly composed of medium to fine fractions, with cumulative passing values of approximately 33 % at 1.00 mm, 67 % at 0.50 mm, and 87 % at 0.16 mm, while finer particles below 0.08 mm account for less than 2 % of the total mass. This controlled granulometry is widely adopted in laboratory studies to minimize variability associated with aggregate grading and to allow direct comparison of mortar performance across different formulations.

The mortar formulations were optimized through the incorporation of a chemical superplasticizer. The superplasticizer employed was MasterCast GT 205, a polycarboxylate ether-based admixture supplied by Master Builders Solutions España S.L.U. The product is characterized by a linear polymer backbone with pendant carboxylate and ether functional groups. According to the manufacturer's technical data, the admixture has a density in the range of 0.870-0.970 g $cm^{-3}$ at 20 °C and an average molecular weight (Mw) of approximately 8000 g $mol^{-1}$ (Navarro-Blasco et al., 2014).

Two commercial phase change materials (PCMs) supplied by MikroCaps (Ljubljana, Slovenia) were used in the mortar formulations in the form of aqueous slurries containing microencapsulated paraffin wax. The first PCM (PCM10-slurry) consists of microcapsules with a paraffin core exhibiting a melting temperature range of approximately 4-10 °C. The slurry contains 25-30 wt% PCM, corresponding to an active PCM content of about 75-80 wt% in the dried microcapsules, with a solid content of 34-38 wt% in the aqueous dispersion. According to the manufacturer, PCM10-slurry provides a latent heat storage capacity of 30-42 J $g^{-1}$ in the slurry and exceeding 110 J $g^{-1}$ in the dried microcapsules. The second PCM (PCM25-slurry) is based on a similar microencapsulation technology but is designed for higher temperature applications, with a melting range of approximately 22-26 °C. This material exhibits a PCM content of 25-30 wt% in the slurry and 75-80 wt % in the dry capsules, a solid content of 35-38 wt% in the dispersion, and a latent heat storage capacity of 150-170 J $g^{-1}$ for the dried microcapsules. The use of slurry-based microencapsulated PCMs facilitated homogeneous dispersion within the mortar matrix while preventing leakage during phase transitions.

### 2.2. Methods

#### 2.2.1. Mortar preparation

Lime-based composite mixtures were designed and produced at laboratory scale, with their compositions summarized in Table 1. All formulations were prepared using a constant binder-to-aggregate (b/a) mass ratio of 1:3.5 and a water-to-binder (w/b) ratio of 0.59, in accordance with guidelines established in previous studies (Groot et al., 2022; Dimou et al., 2022). It should be noted that the PCMs were supplied as aqueous dispersions with a dry content of approximately 35 wt% for both PCM10 and PCM25, the remaining fraction corresponding to water. The water contributed by the PCM dispersions was accounted for in the calculation of the effective water-to-binder (w/b) ratio. The mortars were formulated using air lime, standardized CEN sand, natural pozzolana, white Portland cement, microencapsulated phase change materials, and a polycarboxylate ether-based superplasticizer.

For practical interpretation, the mix compositions were additionally expressed in kg/m$^3$ using the absolute-volume method as described in ASTM C188-77 (Standard Test Method, 2023). True densities of the dry constituents were experimentally determined, while the densities of liquid admixtures (PCM slurries) were obtained from mass-to-volume measurements. The resulting values represent theoretical compositions and are provided to facilitate reproducibility and comparison with conventional volumetric mix designs (Table 2).

The use of two PCMs with different phase-change temperature ranges was deliberately explored to extend the effective thermal buffering window of the rendering mortar. PCM10 (ca. 4-10 °C) is primarily activated during colder conditions and night-time temperature drops, contributing to the moderation of low-temperature fluctuations, while PCM25 (ca. 22-26 °C) targets the typical indoor comfort range and daytime overheating. The hybrid formulation combining both PCMs was designed to assess whether a broader and more continuous latent heat activation could be achieved within a single material, better reflecting real diurnal and seasonal temperature variations encountered by building envelopes. The selected phase-change temperatures are representative of relevant thermal thresholds for building operation in temperate climates and are consistent with values commonly reported in the literature for passive thermal regulation applications.

Dry constituents were first homogenized for 5 min using a laboratory-scale mixer to ensure uniform distribution of the binder components and aggregates. Subsequently, the PCMs (in slurry form) and the pre-determined mixing water were gradually introduced while mixing at low speed until a homogeneous mixture was obtained. The superplasticizer was added progressively, in small increments, to regulate the rheological behaviour of the mortars. Final consistency was verified through standardized flow-table testing in accordance with EN 1015-3 (Methods, 1999), targeting a workability spread of 160 ± 5 mm.

Specimens for laboratory characterization were cast immediately after mixing. Disk-shaped samples (Ø = 55 mm) with thicknesses of 20 mm were prepared for thermophysical testing, while cylindrical specimens (Ø = 30 mm, h = 40 mm) were produced for mechanical characterization. Identical cylindrical specimen dimensions have been adopted in our previous investigations on lime-based composite mortars and thermally enhanced rendering materials (Rubio-Aguinaga et al., 2024a, 2025b), supporting their suitability and ensuring methodological consistency with earlier studies. For thermal efficiency monitoring, the fresh mixtures were cast into rectangular specimens measuring 90 × 180 mm with a thickness of 20 mm and cured under the same controlled laboratory conditions. All specimens were cured under controlled laboratory conditions at 20 ± 2 °C and relative humidity >95%.

At selected curing ages, hydration and carbonation reactions were halted by freeze-drying, involving rapid immersion in liquid nitrogen followed by sublimation at −40 °C under 1 Pa vacuum for 24 h, in order to preserve the microstructural features of the hardened mortars for subsequent analysis (Rubio-Aguinaga et al., 2024a).

#### 2.2.2. Particle size distribution

The particle size distribution of the principal constituents used in this study was determined by laser diffraction using a Malvern Mastersizer instrument (Malvern Panalytical Ltd., UK). The analyzed materials included the PCMs slurries supplied by MikroCaps, tested in their as-received dispersion form, as well as the natural pozzolana and white cement employed are presented in Fig. 1. The volume-weighted mean diameter (D (Tripathi and Shukla, 2024; Baccega and Bottarelli, 2025)) was approximately 10.29 μm for the PCM10-slurry and 11.06 μm for the PCM25-slurry, indicating a comparable microcapsule size range for both PCM systems. For the mineral constituents, D (Tripathi and Shukla, 2024; Baccega and Bottarelli, 2025) values of 8.55 μm and 16.07 μm were obtained for the natural pozzolana and white cement, respectively, reflecting their distinct granulometric characteristics within the composite binder matrix.

#### 2.2.3. Microstructural characterization: scanning electron microscopy and mercury intrusion porosimetry

The microstructural features of the mortar specimens were examined by scanning electron microscopy (SEM) using a COXEM EM-30N instrument (COXEM Co. Ltd., Daejeon, South Korea). Imaging was performed employing a secondary electron (SE) detector, allowing detailed observation of surface morphology within the hardened matrix. Elemental analysis was carried out by energy-dispersive X-ray spectroscopy (EDS) using a Quantax Compact30 system (Bruker Corporation, Billerica, MA, USA), with spectra processed using Esprit Compact software. Prior to SEM observation, specimens were sputter-coated with a thin gold layer using a COXEM SPT-20 ion sputter coater to enhance electrical conductivity and improve image quality.

The pore structure of the rendering mortars and the influence of PCM incorporation were assessed by mercury intrusion porosimetry (MIP). Measurements were conducted using a Micromeritics AutoPore IV 9500 porosimeter (Micromeritics Instrument Corp., Norcross, GA, USA), operating over an applied pressure range from 0.0015 to 207 MPa (ca. 0.2-30000 psia). To ensure representative and reproducible results, analyses were performed on cubic mortar fragments with an approximate edge length of 1 cm.

#### 2.2.4. Capillary water absorption behaviour

Capillary water absorption measurements were carried out on cylindrical mortar specimens using water as the wetting liquid, in accordance with the methodology proposed by Hall and Hoff (2002) and the procedures outlined in EN 1015-18 (Methods of Test, 2002). Prior to

**Table 1**
Mix design of laboratory composites. All quantities were measured by mass.

| No. | Batch | Binder (%) | | | PCMs (%) [a] | | Plasticizer (%) [a] |
|---|---|---|---|---|---|---|---|
| | | Hydrated lime | Natural pozzolan | White cement | PCM10-slurry | PCM25-slurry | |
| 1 | CTRL | 50 | 35 | 15 | - | - | 0.25 |
| 2 | P10-20 | 50 | 35 | 15 | 20 | - | 2.15 |
| 3 | P25-20 | 50 | 35 | 15 | - | 20 | 1.50 |
| 4 | P10/25-10 | 50 | 35 | 15 | 10 | 10 | 1.62 |

[a] in addition by weight to the binder.

**Table 2**
Theoretical mix composition of laboratory composites expressed in kg/m$^3$, calculated by the absolute-volume method and mass-to-volume measurements.

| | Hydrated lime | Natural pozzolan | White cement | Aggregate | Water | PCM10-slurry | PCM25-slurry | Plasticizer |
|---|---|---|---|---|---|---|---|---|
| CTRL | 194.42 | 136.10 | 58.33 | 1360.96 | 229.42 | - | - | 0.97 |
| P10-20 | 176.22 | 123.35 | 52.87 | 1233.52 | 77.03 | 201.39 | - | 7.58 |
| P25-20 | 177.55 | 124.28 | 53.26 | 1242.82 | 77.61 | - | 202.91 | 5.33 |
| P10/25-10 | 176.96 | 123.87 | 53.09 | 1238.69 | 77.35 | 101.12 | 101.12 | 5.73 |

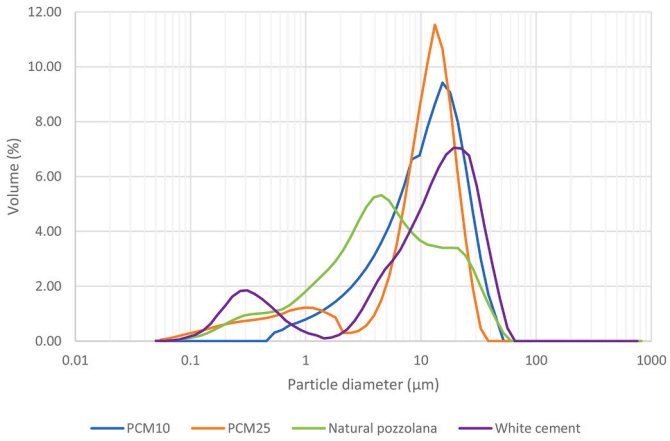


**Fig. 1.** Particle size distribution curves of PCM slurries, natural pozzolana, and white cement.

testing, specimens were dried to constant mass to minimize the influence of residual moisture. During the test, the base of each specimen was placed in contact with water, and the mass increase due to capillary uptake was recorded at predefined time intervals. The capillary absorption coefficient was subsequently determined from the linear relationship between cumulative water uptake per unit area and the square root of time, providing a quantitative measure of the capillary transport behaviour of the mortars.

### 2.2.5. *Mechanical performance: compressive strength*

The compressive strength of the hardened mortars was determined testing the cylinder specimens described above in a Frank/Controls 81565 hydraulic testing press equipped with a Proeti ETI 26.0052 compressive loading device. Tests were conducted under controlled loading conditions, with applied loading rates ranging from 20 to 50 N s$^{-1}$, resulting in a total loading duration between 30 and 90 s, in accordance with standard testing practices. Compressive strength measurements were performed at curing ages of 28, 91, and 182 days to monitor the development of mechanical performance over time. For each formulation and testing age, three cylindrical specimens were tested to ensure statistical reliability and representativeness of the results.

### 2.2.6. *Thermal behaviour: differential scanning calorimetry (DSC), thermal conductivity, and thermal efficiency*

The thermal performance of the mortars was evaluated using three complementary experimental approaches: (i) differential scanning calorimetry (DSC), (ii) thermal conductivity measurements, and (iii) laboratory-scale hot-box testing. DSC analyses were performed to characterize the thermal behaviour of the PCM-enhanced mortars, with particular emphasis on the latent heat of melting ($\Delta H_m$) and crystallization ($\Delta H_c$), as well as the corresponding phase-change temperatures, namely melting temperature ($T_m$) and crystallization temperature ($T_c$). Measurements were carried out using a DSC 25 instrument (TA Instruments, USA), and the resulting data were processed using TRIOS software.

Each specimen was subjected to three consecutive heating-cooling cycles within a temperature range of 20 to 50 °C, using heating and cooling rates of 5 °C·min$^{-1}$. To minimize the influence of prior thermal history and to ensure thermal equilibrium before and after each dynamic segment, isothermal steps of 5 min were introduced at the beginning and end of each cycle. This testing protocol is commonly adopted in DSC investigations of PCM-containing materials to improve the accuracy and reproducibility of phase transition parameters (Rubio-Aguinaga et al., 2024a; Gao et al., 2024). The samples were tested as monolithic fragments, without lids, in order to preserve their macroscopic structure. All DSC measurements were conducted under a nitrogen atmosphere, with a sample purge flow rate of 50 mL min$^{-1}$ and an auxiliary nitrogen flow of approximately 400 mL min$^{-1}$, ensuring stable and reproducible thermal conditions.

Thermal conductivity ($\lambda$) was determined using a FOX50 heat flow meter (TA Instruments, USA), which operates with two independently controlled Peltier elements to impose a constant temperature gradient of 10 °C across the specimens. Disk-shaped samples with a diameter of 55 mm and thicknesses of 20 mm were tested. Measurements were performed at mean specimen temperatures of 5, 15, 25, and 35 °C (defined as the average of the hot and cold plate temperatures) in order to capture the thermal conductivity of the mortars in temperature ranges corresponding to both the solid and liquid states of the incorporated PCMs. Thermal conductivity measurements were performed on specimens cured for 28, 91, and 182 days, allowing assessment of the influence of curing time and microstructural evolution on thermal performance. Reported thermal conductivity values correspond to mean values, with standard deviations calculated from repeated measurements across the investigated temperature range.

The thermal efficiency of the PCM-enhanced mortars was further evaluated using a laboratory-scale hot-box experimental setup designed to reproduce realistic thermal boundary conditions, in line with methodologies reported in previous studies (Rubio-Aguinaga et al., 2025b; Illampas et al., 2021; Shadnia et al., 2015; Young et al., 2018). A single flat mortar specimen (9 × 18 cm, 2 cm thick) was mounted on one side of a thermally insulated expanded polystyrene enclosure (Fig. 2a). The specimen was sealed along its perimeter using high-temperature-resistant silicone to minimize unintended heat losses and to ensure that heat transfer occurred predominantly through the mortar surface rather than through the insulated walls of the enclosure. This configuration enabled one-dimensional heat transfer through the mortar slab, simulating a unidirectional heat exchange scenario representative of wall elements.

Two identical hot-box assemblies were exposed to cyclic thermal loading within a climatic chamber, with temperatures varying between −10 °C and 50 °C and relative humidity ranging from 0% to 60% in order to simulate extreme outdoor conditions (Fig. 2b). A total of four thermal cycles were applied during the testing period. One assembly incorporated a PCM-enhanced mortar specimen, while the second served as a reference system containing a PCM-free mortar. Type-K thermocouples were positioned inside each hot-box enclosure as well as within the climatic chamber to continuously monitor temperature variations. The recorded data were used to evaluate the capacity of the PCM-modified mortars to attenuate temperature fluctuations and regulate heat transfer relative to the reference configuration.

For each configuration, the internal air temperature of the hot-box and the climatic chamber temperature were continuously monitored using calibrated thermocouples connected to a centralized data

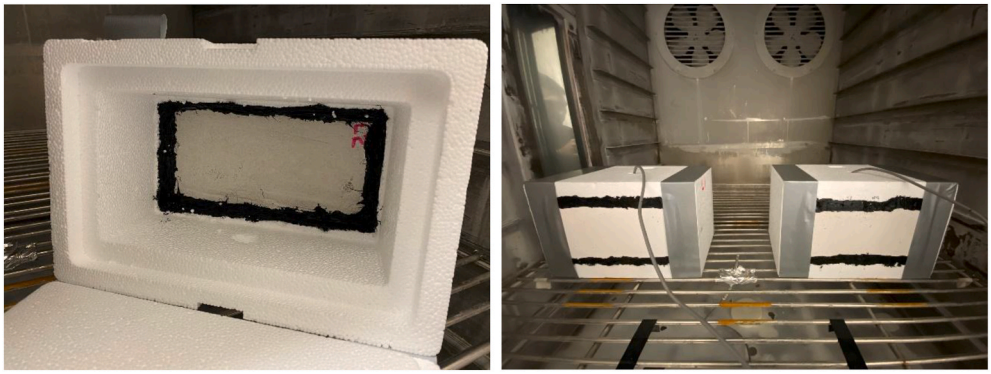

**Fig. 2.** (a) Detailed view of the hot-box interior illustrating the mortar slab sealed with high-temperature-resistant silicone; (b) Experimental arrangement of the hot-box setup inside the climatic chamber, showing the PCM-free and PCM-enhanced configurations.

acquisition system. Three PCM-enhanced mortars (P10-20, P25-20, and P10/25-10) were tested in parallel with a PCM-free reference mortar (CTRL) under identical boundary conditions, allowing direct comparison of their thermal response.

Thermal efficiency was quantified by analysing the attenuation of internal temperature oscillations induced by PCM incorporation. For each heating-cooling cycle, the peak-to-peak temperature amplitude (ΔT) was calculated as in Eq. (1):

$$\Delta T = T_{max} - T_{min} \tag{1}$$

where $T_{max}$ and $T_{min}$ represent the maximum and minimum internal hot-box temperatures recorded during a given cycle. The temperature oscillation reduction attributable to PCM incorporation ($\Delta T_{red}$) was then determined relative to the reference mortar as in Eq. (2):

$$\Delta T_{red} = \Delta T_{CTRL} - \Delta T_{PCM} \tag{2}$$

This approach enables a quantitative assessment of the thermal buffering capacity of the PCM-enhanced mortars by directly comparing their ability to mitigate temperature extremes under dynamic thermal loading.

### 2.2.7. Durability assessment through accelerated ageing tests

The long-term durability of the mortar formulations was evaluated through a series of accelerated ageing tests designed to simulate aggressive environmental conditions commonly encountered in service. Two complementary testing protocols were employed to assess resistance to physical and chemical degradation mechanisms, namely freeze-thaw cycling and salt crystallization.

Freeze-thaw resistance was investigated by subjecting the specimens to 28 consecutive cycles, each consisting of two stages. In the first stage, samples were fully immersed in water for 24 h at ambient temperature to achieve complete saturation. In the second stage, the saturated specimens were transferred to a controlled freezer (Samsung RZ80FJSW) and exposed to a temperature of −20 °C for 24 h to induce freezing. This two-step cycle was repeated continuously for up to 28 cycles or until visible deterioration of the specimens was observed.

Resistance to salt crystallization was assessed by exposing the specimens to cyclic magnesium sulphate attack. Samples were immersed in a saturated $MgSO_4$ solution at 20 °C and 95 % relative humidity for 24 h, followed by oven drying at 110 °C for 18 h. The procedure was continued for a maximum of 28 cycles or until significant degradation was detected.

For all durability tests, cylindrical specimens with dimensions of 30 mm in diameter and 40 mm in height were prepared. Each test was conducted on three replicate specimens per mortar formulation to ensure repeatability and reliability of the results. Throughout the testing programme, specimen mass was recorded at each cycle to quantify material loss or gain and to provide a quantitative indication of damage progression.

In addition to mass measurements, qualitative assessments were performed at regular intervals to visually monitor the evolution of deterioration. Damage was classified using a standardized ten-level damage scale previously developed by Rubio-Aguinaga et al. (2025b) (Table 3), which accounts for the distinct deterioration patterns induced by different ageing mechanisms. Representative photographs corresponding to each damage level were used to document the progression from intact specimens to those exhibiting severe degradation, providing complementary insight into the durability behaviour of the mortars under accelerated ageing conditions.

### 2.2.8. Multi-criteria performance evaluation of ternary mortars using a modified property method

To support the systematic selection of the most suitable PCM-enhanced mortar formulation for external rendering applications, a multi-criteria decision-making approach based on a modified weighting property method was adopted, following methodologies previously proposed for materials selection in engineering (Kaur et al., 2026; Kadhim et al., 2011). This approach enables the integration of heterogeneous experimental results into a unified comparative framework while explicitly accounting for the relative importance of each property with respect to the intended application. The method combines thermophysical, durability, microstructural, and mechanical performance indicators, allowing a balanced evaluation of multifunctional mortars designed primarily for thermal enhancement rather than structural capacity.

The performance criteria considered in this analysis were latent heat storage capacity, thermal conductivity, thermal buffering effectiveness derived from hot-box experiments and expressed as temperature fluctuation (ΔT), freeze-thaw resistance, salt crystallization resistance, capillary water absorption coefficient, and compressive strength. Each property was assigned a relative importance score on a discrete scale from 1 (lowest importance) to 5 (highest importance), reflecting its relevance to the targeted use as an external rendering mortar for thermal retrofitting. Greater weight was attributed to thermal performance indicators, while mechanical strength was assigned lower importance due to the non-structural role of the material. The assigned importance scores were converted into normalized weighting factors ($\alpha_i$) by dividing each score by the sum of all scores, according to Eq. (1):

$$\alpha_i = \frac{w_i}{\sum_{i=1}^{n} w_i} \tag{1}$$

where $w_i$ represents the importance score of property $i$ and $n$ the total number of properties considered.

To enable direct comparison between properties expressed in different units and numerical ranges, the experimentally measured values were normalized using a dimensionless scaling procedure. For

**Table 3**
Damage scale and visual assessment of durability tests (Rubio-Aguinaga et al., 2025b).

| Damage scale | Characteristics |
|---|---|
| 0 | No visible damage; specimen intact |
| 1 | Minimal material loss; almost no damage |
| 2 | Small cracks; slight material loss |
| 3 | Moderate cracks; visible wear |
| 4 | Larger cracks; significant material loss |
| 5 | Major cracks; pronounced material loss |
| 6 | Severe cracks; surface starting to break apart |
| 7 | Large sections missing; extensive cracking |
| 8 | Structure heavily compromised; crumbling |
| 9 | Near total destruction; disintegration visible |
| 10 | Total destruction; specimen turned to dust |

properties where higher values correspond to improved performance, such as latent heat storage, thermal buffering efficiency, mechanical strength, and durability indicators, the scaled value ($\beta_i$) was calculated as in Eq. (2):

$$\beta_i = \frac{X_i}{X_{i,max}} \times 100 \quad (2)$$

Conversely, for properties where lower values indicate superior performance, including thermal conductivity and capillary absorption, an inverse normalization was applied using Eq. (3):

$$\beta_i = \frac{X_{i,min}}{X_i} \times 100 \quad (3)$$

where $X_i$ is the measured value for a given formulation, and $X_{i,max}$ or $X_{i,min}$ represent the maximum or minimum values observed among all formulations for that specific property. This normalization ensured that all criteria contributed on a comparable basis without bias toward parameters with larger numerical magnitudes.

For each mortar formulation, the weighted contribution of each property was calculated as the product of the weighting factor and the normalized performance value. The overall performance index ($I$) was then obtained by summing the weighted contributions of all considered properties using Eq. (4):

$$I = \sum_{i=1}^{n} (\alpha_i \cdot \beta_i) \quad (4)$$

The resulting performance index provides a single quantitative measure of the global suitability of each formulation for the defined application scenario. At the same time, the relative contributions of individual properties allow assessment of how thermal, durability, and physical characteristics influence the overall ranking. This approach supports transparent and application-oriented decision-making, particularly for PCM-enhanced lime-based mortars, where optimizing thermal functionality must be balanced against durability, microstructure, and acceptable mechanical performance.

#### 2.2.9. *Assessment of the performance under real exposure conditions: Algete pilot site and mock-up configuration*

Field-scale validation of the PCM-enhanced lime-based rendering mortar was conducted at the Algete DemoPark (Madrid, Spain), an outdoor experimental facility operated by ACCIONA and dedicated to the evaluation of innovative construction materials under real environmental conditions. The pilot consists of full-scale, adiabatic test cells designed to reproduce façade-level heat transfer while minimizing lateral and rear thermal losses. This configuration allows controlled comparison of alternative retrofit solutions exposed to identical climatic conditions.

Within the present study, the analysis was limited to two mock-ups: a reference configuration (Reference) and a PCM-enhanced configuration (Mockup-3) (see Fig. 3 and Fig. 4). Both mock-ups employed prefabricated hempcrete masonry blocks (PAL 15, IsoHemp S.A.-N.V.), with nominal dimensions of 60 × 30 cm and a thickness of 15 cm, as the baseline substrate. These blocks were selected for their low density, high vapour permeability, and suitability for sustainable and bio-based building envelope applications.

In the reference mock-up, the hempcrete walls were finished with a commercially available cement-based render (Planitop Fast 330, Mapei S.p.A.), applied without the incorporation of phase change materials. The rendering system was executed on the east-, west- and south-facing walls of the mock-up and consisted of two successive layers, with an embedded basalt fibre reinforcement mesh (MAPEGRID B 250, mesh size 6 × 6 mm) placed between the layers to improve mechanical performance and crack control. The total render thickness was approximately 2 cm, and this configuration served as the baseline system for comparison.

In contrast, Mockup-3 incorporated a ternary lime-pozzolan-cement render corresponding to mixture P25-20 (Table 1), containing microencapsulated phase change materials with a nominal phase-change temperature of 25 °C. The PCM-enhanced render was applied following the same construction methodology as the reference system, namely two-layer application with an intermediate basalt reinforcement mesh (MAPEGRID B 250) and a total thickness of approximately 2 cm, on the east-, west- and south-facing walls of the mock-up.

By maintaining identical substrate characteristics, reinforcement strategy, layer configuration, orientation, and application thickness in both mock-ups, the experimental design ensured that any observed differences in thermal behaviour could be attributed primarily to the incorporation of PCMs, rather than to construction or geometric variables.

Both mock-ups were instrumented with an identical sensor layout to enable direct comparison of thermal response. Monitoring focused on the east and west façades, which were selected for detailed thermal assessment under real exposure conditions. Thermocouples were installed at selected locations within the wall assemblies as well as within the interior of each mock-up to continuously record temperature

**Fig. 3.** Pilot-scale mock-ups with hempcrete baseline, illustrating the construction stages: application of the external rendering system on the hempcrete substrate and the final appearance of the hardened mortar layer on the external façade.

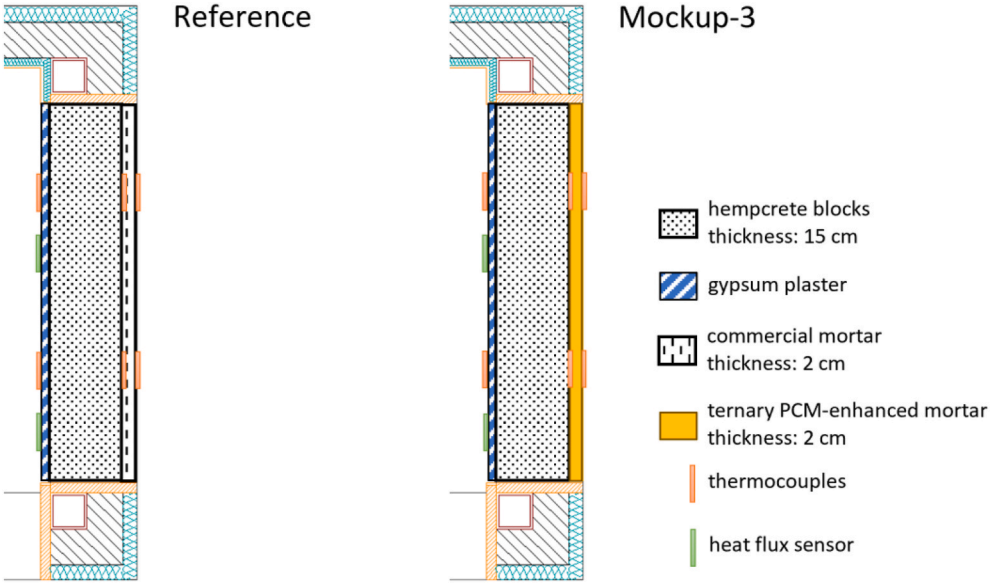


**Fig. 4.** Schematic cross-section of the reference and PCM-enhanced wall assemblies illustrating sensor placement.

evolution (Fig. 3 and Fig. 4). In addition, heat flux sensors were positioned on the internal side of the wall, co-located with the temperature sensors. These sensors measured the instantaneous heat flux ($W \cdot m^{-2}$) crossing the wall section, providing information on both the magnitude and direction of heat transfer between the exterior environment and the interior space; positive and negative values correspond to heat gains and heat losses, respectively.

A further monitored parameter was the interior air temperature recorded by a THL (Temperature-Humidity-Light) sensor installed at the centre of the mock-up enclosure. Although the device provides multiple environmental variables, only the temperature signal was considered in the present study. This measurement represents the freely circulating indoor air temperature within the enclosure and is independent of the thermocouples embedded in or attached to the wall assemblies. As such, it provides complementary information on the overall thermal conditions inside the mock-up, integrating the combined effects of heat transfer through the envelope and air heat accumulation within the enclosed space. The THL temperature is therefore used as a qualitative indicator of the global thermal response of the wall-enclosure system under dynamic external conditions, rather than as a direct measure of wall heat transfer.

Additional sensors were deployed to monitor ambient outdoor conditions within the DemoPark, including air temperature and relative humidity, thereby providing the necessary boundary conditions for data interpretation. All sensors were integrated into a Grafana cloud-based monitoring platform, allowing real-time data logging, synchronization, and long-term visualization of the thermal and environmental parameters.

The monitoring campaign focused on capturing the dynamic thermal behaviour of the wall assemblies under natural diurnal temperature fluctuations. Particular attention was given to temperature attenuation and time-shift effects associated with the PCM-enhanced render relative to the PCM-free reference configuration. The Algete pilot thus served as an intermediate validation scale, bridging laboratory characterization and real-world application conditions.

## 3. Results and discussion

### 3.1. Characterization of the mortars

#### 3.1.1. Assessment of the microstructure

Scanning electron microscopy was employed to examine the morphology of the lime-based mortars and to assess how the inclusion of microencapsulated phase change materials influences the binder

microstructure. The reference mortar exhibits a typical lime-cement matrix characterized by an irregular pore network and mineral phases forming a continuous framework (Fig. 5a). In contrast, PCM-modified mortars show the systematic presence of spherical inclusions embedded within the matrix, attributable to the microencapsulated PCM particles (Fig. 5b–d).

Across all PCM-containing formulations, these spherical inclusions appear well preserved within the hardened matrix, with no visual indications of shell fragmentation or collapse (Fig. 6). The microcapsules remain clearly distinguishable from the surrounding binder, suggesting that the encapsulation system withstands the mechanical and physicochemical conditions associated with mortar preparation and curing. Their stable appearance within the matrix indicates that PCM incorporation does not introduce microstructural damage at the scale observable by SEM. In certain regions, due to specimen fracture in those areas, some of the microcapsules have been lost, leaving only the residual void observable.

The distribution of the microcapsules within the lime matrix appears spatially consistent, with no regions exhibiting excessive accumulation of PCM capsules. This spatial regularity implies that the presence of PCMs does not disrupt the rheological stability of the fresh mortar to an extent that would promote segregation or localized concentration effects. Instead, the capsules are incorporated as discrete inclusions within the existing pore-binder framework.

At the capsule-matrix interface, the lime binder conforms closely to the microcapsule surfaces, indicating effective physical embedding. Such intimate contact suggests favorable conditions for thermal exchange between the PCM core and the surrounding matrix while preserving the continuity of the mineral skeleton. Taken together, the SEM observations indicate that the microencapsulated PCMs are successfully integrated into the lime-based mortars, modifying the internal architecture without compromising the structural coherence of the binder system.

In order to further support the microstructural observations, SEM analysis was complemented by energy-dispersive X-ray spectroscopy (EDS), enabling the correlation of morphological features with their elemental composition. EDS mapping analyses confirmed the compositional contrast between the lime-based matrix and the PCM microcapsules. The surrounding binder matrix is predominantly composed of calcium-rich phases, associated with lime hydration and carbonation products (Fig. 6b), while the microcapsules exhibit a distinct elemental signature characterized by lower calcium content (Fig. 6d) and the presence of elements associated with the polymeric shell and organic PCM core (Fig. 6c). This compositional differentiation supports the identification of the spherical inclusions as microencapsulated PCM particles.

At the capsule-matrix interface, EDS results indicate a clear boundary between the inorganic binder and the organic microcapsule, with no evidence of chemical interaction or degradation of the capsule shell. This observation further confirms that the microencapsulation system remains stable during mortar preparation and curing, ensuring the effective containment of the PCM within the matrix.

While SEM provides qualitative insight into the morphology and distribution of the PCM microcapsules, quantitative assessment of the pore structure is provided by mercury intrusion porosimetry (MIP). This technique was employed to further elucidate the influence of microencapsulated PCM incorporation on the pore structure of the ternary mortars. The pore size distribution curves for all formulations at different curing ages are presented in Fig. 7a–c, while Fig. 7d provides a comparative breakdown of pore size classes expressed as relative percentages of total porosity. Quantitative values of open porosity and average pore diameter are summarized in Table 4.

The reference mortar (CTRL) exhibits a relatively stable pore structure across curing ages, with open porosity values ranging between 24.3 % and 25.6 % and average pore diameters remaining close to 100 nm. This behaviour is consistent with the progressive densification typically observed in lime-pozzolan-cement systems, where carbonation and secondary hydration reactions lead to gradual refinement of the pore network over time. As shown by the pore size class distribution (Fig. 7d), the CTRL mortar is dominated by pores larger than 200 nm at all curing

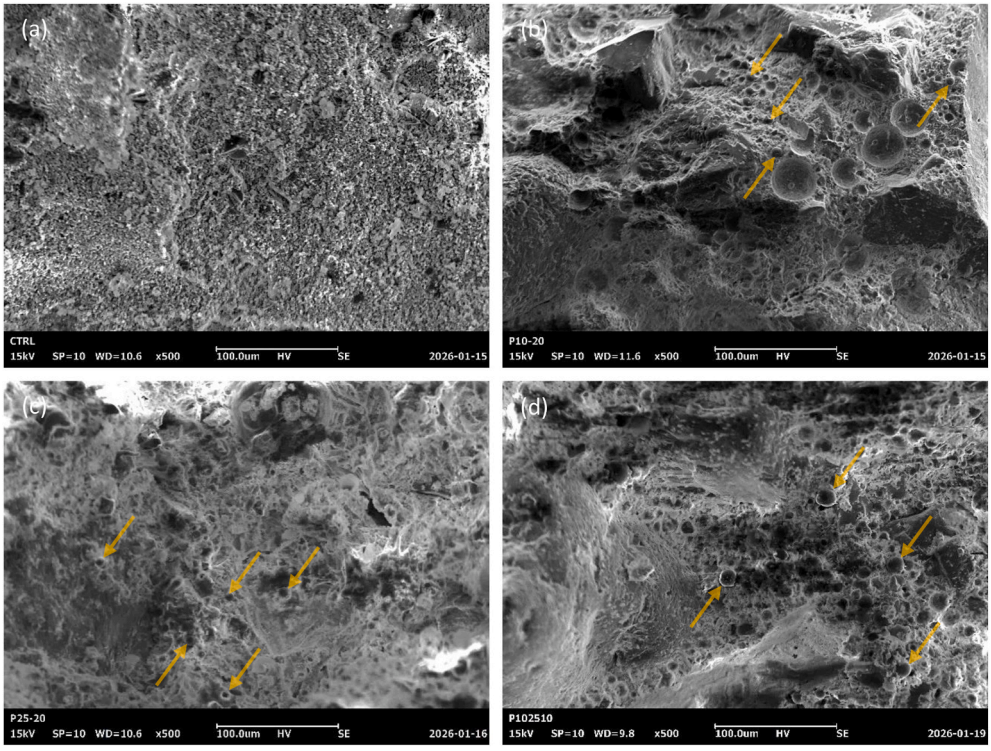


**Fig. 5.** SEM images of ternary mortars: (a) CTRL; (b) P10-20; (c) P25-20; and (d) P10/25-10. Yellow arrows indicate representative spherical PCM microcapsule inclusions embedded within the binder matrix.

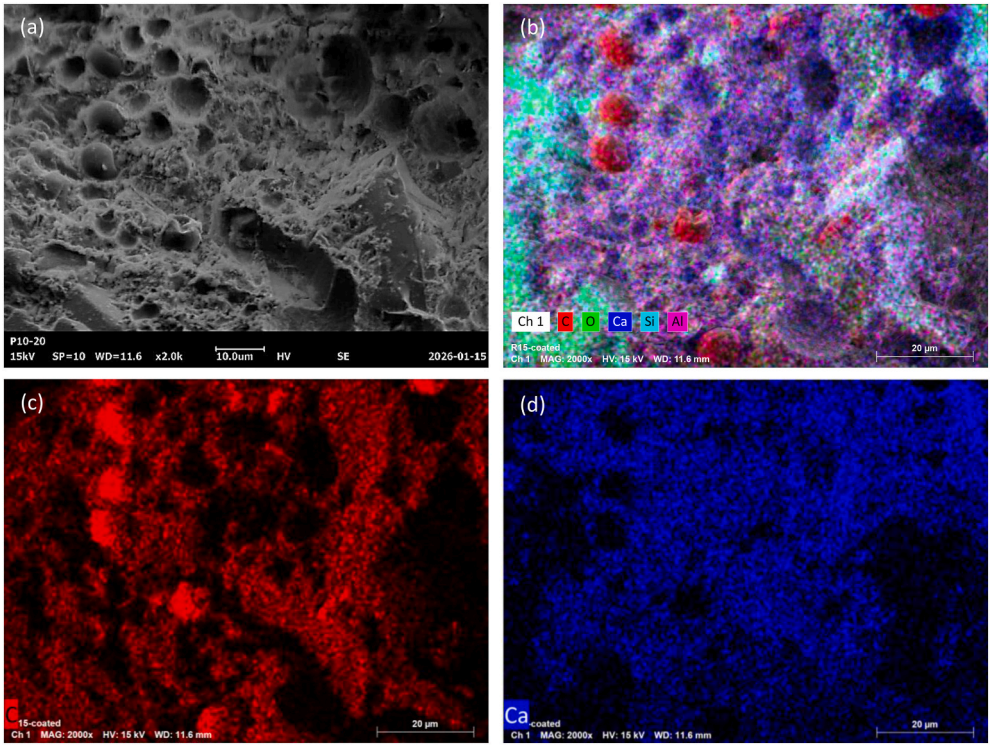


**Fig. 6.** SEM analysis of sample P10-20: (a) SEM micrograph showing the material's microstructural features; (b) EDS multi-element mapping; (c) EDS carbon mapping; (d) EDS calcium mapping.

ages, with comparatively limited contributions from finer pore fractions, indicating a relatively coarse but stable pore network.

The incorporation of PCM-containing slurries results in measurable modifications to the pore structure, the extent of which depends on both PCM type and formulation. At 28 days, the mortar containing PCM10 at 20 wt% (P10-20) displays a slightly reduced open porosity compared to the reference (23.1 %), accompanied by a modest increase in average pore diameter. At this age, Fig. 7d shows a redistribution of porosity from the >200 nm class towards the 20-50 nm range. However, at 91 days, P10-20 shows a pronounced increase in open porosity (32.5 %) and a corresponding increase in average pore diameter (126.9 nm), indicating a temporary coarsening of the pore network during intermediate curing stages. By 182 days, both porosity and average pore size decrease towards values comparable to the reference mortar, suggesting a partial reorganization and stabilization of the matrix as curing progresses. This evolution is mirrored by a reduction in the proportion of large pores and a more balanced distribution across pore size classes.

A more pronounced effect on pore size distribution is observed in the mortar incorporating PCM25 at 20 wt% (P25-20). At early curing age (28 days), this formulation exhibits a substantially higher average pore diameter (192.0 nm) compared to the reference, despite maintaining open porosity values within a similar range. This shift towards larger pore sizes is clearly reflected in the pore size distribution curves (Fig. 7a–c), and further confirmed by Fig. 7d, which shows an increased contribution of pores greater than 200 nm at early age. With increasing curing time, the pore structure progressively refines, as evidenced by the decrease in average pore diameter to 157.8 nm at 91 days and further to 92.5 nm at 182 days. This refinement is accompanied by a redistribution of porosity toward the intermediate pore range (50-200 nm), indicating gradual densification of the binder matrix.

The hybrid formulation containing both PCM10 and PCM25 at 10 wt % each (P10/25-10) exhibits intermediate behaviour. At 28 and 91 days, this mortar presents higher open porosity and average pore diameter compared to the reference, consistent with a broader pore size distribution resulting from the coexistence of two PCM systems. The pore size class analysis (Fig. 7d) highlights a relatively balanced distribution between intermediate and larger pores at early and intermediate ages. Nevertheless, by 182 days, a marked reduction in average pore diameter (59.3 nm) is observed, accompanied by a decrease in open porosity. This late-age refinement is associated with an increased proportion of pores in the <20 nm range and a reduced contribution of large pores, suggesting improved packing efficiency and progressive accommodation of the microcapsules within the evolving binder matrix.

Overall, the MIP results indicate that PCM incorporation influences the pore structure primarily through a redistribution of pore sizes, rather than by inducing a systematic increase in total open porosity. At early and intermediate curing stages, PCM addition tends to promote a shift toward larger and intermediate pores, the magnitude of which depends on PCM type and formulation. Importantly, the tendency toward pore refinement at longer curing times demonstrates that the lime-based composite matrix is capable of adapting to the presence of microencapsulated PCMs, mitigating initial microstructural disturbances associated with PCM incorporation.

These observations are consistent with the microstructural evidence obtained from SEM analysis, which showed that PCM addition does not induce significant microstructural damage or disruption of the lime matrix. Instead, the presence of microcapsules is primarily reflected in controlled changes to the pore size distribution and total accessible porosity, rather than in the formation of microcracks or discontinuities. From a materials performance perspective, the observed variations in open porosity remain within a moderate range and do not compromise the continuity of the binder framework, indicating that the selected PCM dosages are compatible with ternary lime-cement mortars intended for rendering applications.

### *3.1.2. Capillary water absorption behaviour*

The capillary water absorption coefficients of the reference and PCM-enhanced mortars at curing ages of 28, 91, and 182 days are presented in Fig. 8. The results show a clear differentiation between the reference mortar and the PCM-containing formulations, with PCM incorporation

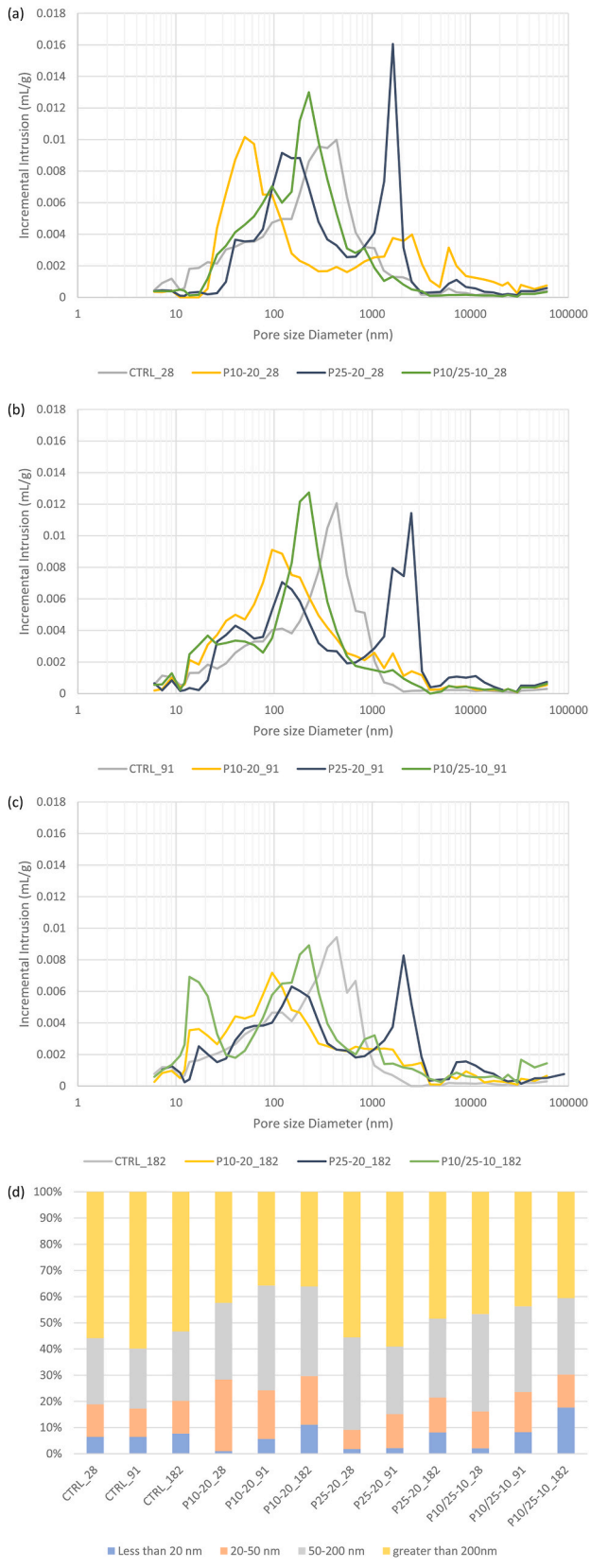


**Fig. 7.** Pore size distribution of ternary mortars measured after (a) 28, (b) 91, and (c) 182 days of curing. Subfigure (d) summarizes the pore structure by reporting the percentage contribution of four pore size ranges (<20 nm, 20–50 nm, 50–200 nm, and >200 nm), normalized to 100%, for all mixtures and curing ages.

**Table 4**
Open porosity and average pore diameter of the mortar formulations as obtained from mercury intrusion porosimetry (MIP) analysis.

| No. | Batch | Open porosity (%) | | | Average pore diameter (nm) | | |
|---|---|---|---|---|---|---|---|
| | | 28d | 91d | 182d | 28d | 91d | 182d |
| 1 | CTRL | 24.3 | 25.6 | 24.4 | 99.4 | 113.3 | 95.8 |
| 2 | P10-20 | 23.1 | 32.5 | 27.4 | 102.9 | 126.9 | 97.2 |
| 3 | P25-20 | 26.7 | 27.0 | 22.1 | 192.0 | 157.8 | 92.5 |
| 4 | P10/25-10 | 27.0 | 29.3 | 24.6 | 138.7 | 119.2 | 59.3 |

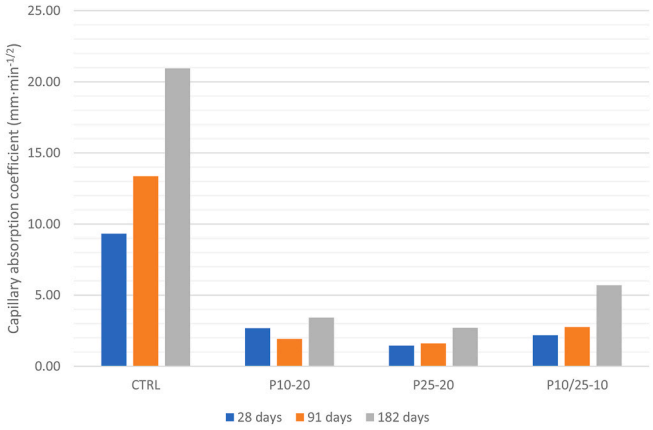


**Fig. 8.** Capillary water absorption coefficient of the reference and PCM-modified ternary mortars measured at 28, 91, and 182 days of curing.

leading to a marked reduction in capillary water uptake at all curing stages.

The reference mortar (CTRL) exhibits the highest capillary absorption coefficients, with values increasing significantly over time, from approximately 9.3 mm $min^{-1/2}$ at 28 days to about 21.0 mm $min^{-1/2}$ at 182 days. This progressive increase suggests increased connectivity of capillary pores as curing advances, which is consistent with the relatively stable average pore size observed in the MIP analysis and indicates the persistence of an interconnected pore network conducive to water transport.

In contrast, all PCM-enhanced mortars display substantially lower capillary absorption coefficients compared to the reference formulation. The P10-20 mortar shows a pronounced reduction in water uptake, with values remaining below 3.5 mm $min^{-1/2}$ across all curing ages. A similar trend is observed for the P25-20 formulation, which exhibits the lowest capillary absorption coefficients among the tested mortars, remaining close to or below 2.5 mm $min^{-1/2}$ even at 182 days. These results indicate a significant mitigation of capillary transport mechanisms due to PCM incorporation.

The hybrid formulation P10/25-10 presents intermediate behaviour, with capillary absorption coefficients higher than those of P10-20 and P25-20 but still markedly lower than the reference mortar. Although an increase in capillary absorption is observed at 182 days, values remain well below those of CTRL, indicating sustained resistance to water ingress.

When interpreted alongside the MIP results, the reduced capillary absorption of PCM-enhanced mortars suggests that PCM incorporation alters not only total porosity but also pore connectivity. Although some PCM-containing formulations exhibited transient increases in average pore diameter at intermediate curing ages, these changes did not translate into enhanced capillary transport, implying that the pore network remains less continuous or more effectively blocked. This behaviour may be associated with the presence of PCM microcapsules and their polymeric shells, which can disrupt continuous capillary pathways within the matrix.

Overall, the capillary absorption results demonstrate that PCM-enhanced lime-based composite mortars exhibit improved resistance to water ingress compared to the reference formulation. This reduction in capillary uptake is particularly relevant for rendering applications, as it may contribute to enhanced durability by limiting moisture-related degradation mechanisms, while remaining compatible with the vapour-permeable nature required for heritage and retrofit contexts.

### 3.1.3. Mechanical performance

The evolution of compressive strength of the mortars was evaluated at curing ages of 28, 91, and 182 days, as shown in Fig. 9. All formulations exhibit a progressive increase in compressive strength with curing time, reflecting ongoing carbonation of the lime matrix and secondary hydration reactions associated with the pozzolanic component and the white cement fraction.

The reference mortar (CTRL) shows a gradual strength development, increasing from approximately 2.9 MPa at 28 days to around 4.3 MPa at 91 days and stabilizing at approximately 4.2 MPa at 182 days. This behaviour is consistent with the relatively stable pore structure observed in the MIP analysis, where both open porosity and average pore diameter remained nearly constant across curing ages, indicating a well-balanced and progressively densifying matrix.

Mortars incorporating microencapsulated PCMs generally exhibit comparable or enhanced compressive strength relative to the reference formulation, depending on PCM type and curing age. The P10-20 mortar displays a clear improvement in mechanical performance compared to CTRL, particularly at later curing ages. Compressive strength increases from approximately 2.7 MPa at 28 days to about 5.1 MPa at 91 days and further to approximately 5.4 MPa at 182 days. This enhancement occurs despite the temporary increase in open porosity and average pore diameter observed at 91 days in the MIP results. The subsequent reduction in pore size and porosity at 182 days suggests progressive microstructural refinement, which likely contributes to the improved mechanical response at longer curing times.

The P25-20 formulation exhibits a more moderate strength development. While compressive strength at 28 days is comparable to that of the reference mortar, values at 91 and 182 days remain slightly lower than those of P10-20 but comparable to or higher than CTRL. This trend is consistent with the MIP observations, which revealed a pronounced increase in average pore diameter at early curing ages for this formulation, followed by a marked reduction at 182 days. The initial coarsening of the pore network associated with the PCM25 incorporation may temporarily limit strength development, while subsequent pore refinement mitigates its long-term impact.

The hybrid PCM formulation (P10/25-10) shows the lowest compressive strength among the PCM-containing mortars at 28 days, with values around 2.3 MPa. However, a substantial increase is observed at 91 and 182 days, reaching values comparable to the reference mortar. This delayed strength development aligns with the MIP results, which indicate higher open porosity and larger average pore diameters at early ages, followed by significant pore refinement at 182 days. The marked decrease in average pore diameter at later curing stages suggests improved matrix continuity, supporting the observed recovery in compressive strength.

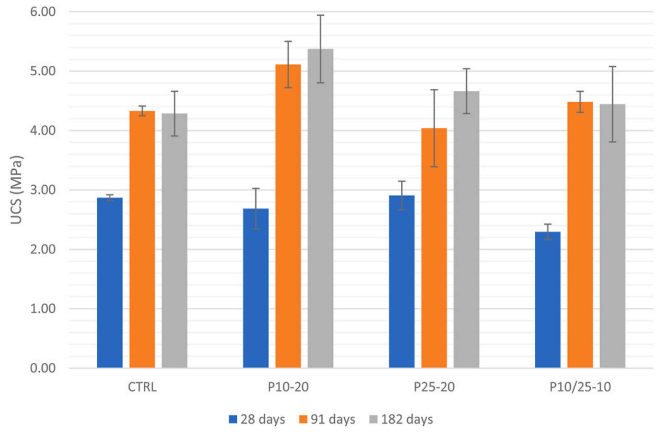


**Fig. 9.** Compressive strength (UCS) of the mortar formulations at 28, 91, and 182 days of curing.

Overall, the compressive strength results indicate that the incorporation of microencapsulated PCMs at the investigated dosages does not inherently compromise the mechanical performance of lime-based composite mortars. Instead, mechanical behaviour appears strongly dependent on the interaction between PCM type, curing time, and microstructural evolution. In particular, transient pore coarsening observed at early and intermediate curing ages does not necessarily translate into long-term mechanical degradation, as the binder matrix progressively adapts and densifies with time.

These findings, in conjunction with the MIP results, highlight the importance of considering time-dependent microstructural development when assessing the mechanical performance of PCM-enhanced mortars. The results suggest that appropriately designed PCM-containing lime-based mortars can maintain, or even enhance, compressive strength while providing additional thermal functionality. Recent studies on microencapsulated PCM-modified lime renders have emphasized that the interaction between PCM microcapsules and chemical additives may significantly influence dispersion, workability, and the resulting microstructural environment (Rubio-Aguinaga et al., 2024b). Such formulation-related factors are critical in controlling porosity and interfacial transition characteristics, and therefore in ensuring a balanced combination of thermal performance and mechanical integrity.

From an application perspective, it is important to note that the investigated mortars are intended for use as rendering materials rather than structural elements. In such applications, compressive strength is not the governing design parameter; instead, sufficient mechanical integrity, adhesion, durability, and compatibility with the substrate are of primary importance. The compressive strength values obtained in this study are consistent with those reported for lime-based rendering mortars. In particular, the 28-day strength values fall within the CS I-CS II categories defined in EN 998-1 (Specification for Mortar, 2018) for rendering and plastering mortars, while the progressive increase observed at later curing ages reflects ongoing carbonation and pozzolanic reactions typical of lime-cement systems. These results indicate that the investigated mortars provide adequate mechanical performance for façade rendering applications, while also offering enhanced thermal functionality.

### 3.1.4. Evaluation of the thermal response of the monolithic specimens

Differential Scanning Calorimetry (DSC) was used to assess the latent heat storage behaviour of the lime-based mortars at 182 days of curing, focusing on the thermal response of the materials in bulk form. The analysis aimed to verify the persistence, activation, and magnitude of phase-change phenomena within the hardened mortar matrix following PCM incorporation. For this reason, DSC thermograms of the reference mortar (CTRL) and the PCM-modified mortars were analyzed.

The normalized DSC heat flow curves obtained during heating and cooling cycles are presented in Fig. 10, while the corresponding phase-change enthalpies and peak temperatures are summarized in Table 5. The reference mortar (CTRL) exhibited no detectable endothermic or exothermic events across the investigated temperature range, confirming the absence of latent heat storage and indicating a purely sensible heat response of the lime-based matrix. In contrast, all PCM-bearing mortars displayed clear endothermic peaks during heating and exothermic peaks during cooling, associated with the melting and crystallization of the embedded microencapsulated PCMs, as expected (Frahat et al., 2023; Hattan et al., 2021). This confirms that the PCMs

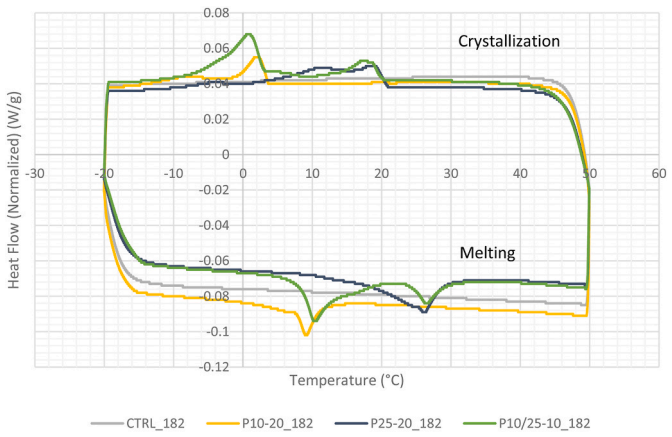


**Fig. 10.** DSC heat-flow curves of laboratory composites at 182 days of curing.

**Table 5**
Latent heat enthalpies and corresponding phase-change peak temperatures obtained from DSC analysis of reference and PCM-modified mortars at 182 days of curing.

| Batch | Enthalpy (J/g) | | Peak temperatures (°C) | |
|---|---|---|---|---|
| | Melting | Crystallization | Melting | Crystallization |
| CTRL | - | - | - | - |
| P10-20 | 0.77 | 1.07 | 9.11 | 2.00 |
| P25-20 | 1.85 | 2.20 | 26.15 | 18.72 |
| P10/25-10 | 2.70 | 2.79 | 10.37 & 26.48 | 0.82 & 17.47 |

remain thermally active within the mortar matrix after 182 days of curing and are capable of reversibly storing and releasing thermal energy.

Quantitative integration of the DSC curves reveals marked differences among the PCM-modified formulations (Table 5). The P10-20 mortar exhibited relatively low latent heat values, with melting and crystallization enthalpies of 0.77 J/g and 1.07 J/g, respectively, and phase-change peaks centred at approximately 9.11 °C during melting and 2.00 °C during crystallization. These results indicate a limited but measurable latent heat contribution, consistent with the lower heat storage capacity of PCM10.

The P25-20 mortar exhibited a markedly higher latent heat storage capacity, with melting and crystallization enthalpies of 1.85 J/g and 2.20 J/g, respectively. The corresponding phase-change peaks were detected at higher temperatures, namely 26.15 °C during melting and 18.72 °C during crystallization, in good agreement with the nominal phase-change temperature range of PCM25. These results indicate a more pronounced and effective latent heat storage contribution at the composite material scale, reflecting a higher thermal energy storage potential associated with the incorporation of PCM25 within the lime-based matrix.

The hybrid formulation P10/25-10 exhibited the highest overall latent heat values, with melting and crystallization enthalpies of 2.70 J/g and 2.79 J/g, respectively. Notably, this mortar displayed multiple phase-change peaks during both heating and cooling, reflecting the coexistence of two PCM systems with distinct transition temperatures. Melting peaks were observed at approximately 10.37 °C and 26.48 °C, while crystallization occurred around 0.82 °C and 17.47 °C. This confirms the design rationale of combining PCMs with different melting points to achieve latent heat storage across multiple temperature intervals relevant to building operation.

This multi-peak behaviour demonstrates that the hybrid PCM mortar is capable of storing and releasing latent heat across a broader and discontinuous temperature range compared to single-PCM systems, effectively extending the window of thermal activity. To the authors' knowledge, this study represents one of the first detailed experimental investigations of mixed-PCM ternary mortars, combining laboratory-scale thermal characterization with microstructural analysis and performance assessment. The results highlight the potential of hybrid PCM formulations as a design strategy for tailoring the thermal response of binding materials, enabling the development of thermally efficient mortars optimized for specific climatic conditions and diurnal temperature profiles.

Importantly, the presence of well-defined and repeatable melting and crystallization peaks after prolonged curing demonstrates the chemical and mechanical stability of the microencapsulated PCMs within the alkaline lime-based matrix. These findings are consistent with previous studies reporting the long-term sustained thermal functionality of PCMs in cementitious and lime-based materials (Rubio-Aguinaga et al., 2024a).

Overall, the DSC results provide clear quantitative evidence that the incorporation of PCMs imparts a stable latent heat storage capacity to lime-based mortars at the bulk material level. Both the magnitude and the temperature range of the enthalpy peaks are strongly dependent on the PCM type and formulation strategy. In particular, the P25-20 mortar benefits from the higher intrinsic heat storage capacity of PCM25, resulting in more pronounced phase-change enthalpies within a temperature range relevant to building applications, while the hybrid formulation exhibits thermal activity distributed across multiple temperature intervals. These findings demonstrate the effective integration and functionality of microencapsulated PCMs within the lime matrix, highlighting their potential to enhance the thermal energy storage capability of lime-based mortars.

Thermal conductivity measurements for the reference and PCM-enhanced mortars at curing ages of 28, 91, and 182 days are presented in Fig. 11. The results indicate that the incorporation of microencapsulated PCMs leads to a systematic reduction in thermal conductivity compared to the reference mortar, with the magnitude of the reduction depending on PCM type and curing age. The reference mortar (CTRL) exhibits the highest thermal conductivity at all ages, with values decreasing from approximately 0.87 W $m^{-1}{\cdot}K^{-1}$ at 28 days to around 0.63-0.65 W $m^{-1}{\cdot}K^{-1}$ at later curing stages, reflecting progressive microstructural evolution and moisture redistribution within the matrix.

All PCM-containing mortars display significantly lower thermal conductivity values than the control formulation. Among them, P10-20 shows the lowest conductivity across curing ages, decreasing from approximately 0.47 W $m^{-1}{\cdot}K^{-1}$ at 28 days to about 0.30 W $m^{-1}{\cdot}K^{-1}$ at 182 days. This pronounced reduction can be attributed to the combined effects of PCM incorporation and microstructural modification, as

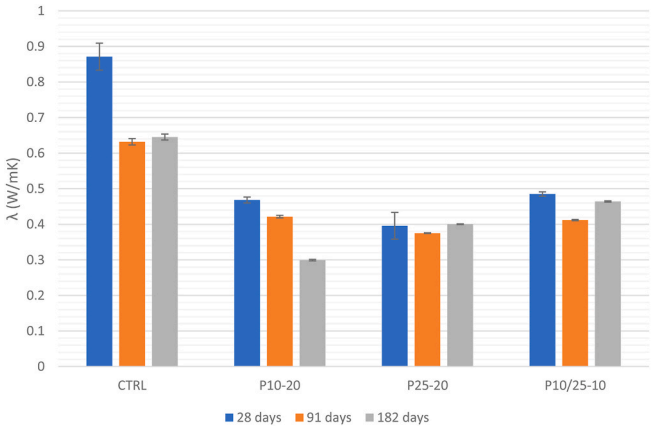


**Fig. 11.** Thermal conductivity (λ) of the reference mortar (CTRL) and PCM-modified mortars (P10-20, P25-20, and P10/25-10) measured at 28, 91, and 182 days of curing. Error bars indicate standard deviation of the measurements across different temperatures.

evidenced by the MIP results, which revealed transient increases in porosity and pore size at intermediate curing ages. The reduced conductivity is consistent with the inherently lower thermal conductivity of the PCM microcapsules compared to the mineral binder phases, as well as with the increased contribution of air-filled pores to heat transfer resistance.

The reduction in thermal conductivity observed in PCM-modified mortars can be attributed to a combination of intrinsic material properties and microstructural effects. The PCM used in this study consists of paraffin-based cores encapsulated within melamine-formaldehyde shells, both of which exhibit lower thermal conductivity compared to the surrounding mineral binder phases (Mitran et al., 2021; Bose and Amirtham, 2016; Peng et al., 2018). In addition, the incorporation of microencapsulated PCM modifies the internal structure of the mortar by introducing dispersed inclusions and increasing porosity, as indicated by SEM and MIP results. These features act to disrupt continuous heat transfer pathways within the matrix, thereby enhancing the overall thermal resistance. Consequently, the observed decrease in thermal conductivity results from the combined influence of the PCM intrinsic properties and the microstructural changes induced by its incorporation.

The P25-20 formulation exhibits intermediate thermal conductivity values, ranging from approximately 0.40 W $m^{-1}{\cdot}K^{-1}$ at 28 days to around 0.38-0.40 W $m^{-1}{\cdot}K^{-1}$ at later ages. Despite the larger average pore diameters observed at early curing stages for this formulation, the thermal conductivity remains relatively stable with time, suggesting that pore size coarsening does not necessarily translate into proportional changes in conductive heat transfer once the matrix reaches a stabilized state. Similarly, the hybrid formulation P10/25-10 shows reduced thermal conductivity compared to CTRL at all curing ages, with values remaining within a narrow range (approximately 0.41-0.48 W $m^{-1}{\cdot}K^{-1}$), indicating a balanced contribution of both PCM types to the thermal response.

Overall, the results demonstrate that PCM incorporation in lime-based composite mortars leads to a meaningful reduction in thermal conductivity without inducing excessive variability with curing time. When considered together with the MIP and compressive strength results, these findings indicate that the reduction in thermal conductivity is primarily associated with PCM incorporation and associated microstructural adjustments, rather than with changes in matrix integrity. Importantly, the reduced thermal conductivity complements the latent heat storage functionality of the PCMs, enhancing the potential of these mortars to contribute to thermal regulation in building envelope applications while maintaining adequate mechanical performance.

### 3.1.5. *Thermal efficiency of the mortars in lab-scale pilots*

The thermal efficiency of the reference and PCM-enhanced mortars was further assessed through laboratory-scale hot-box experiments subjected to cyclic thermal loading, simulating pronounced diurnal temperature variations. Fig. 12a–c compares the internal temperature evolution of the hot-boxes incorporating the reference mortar (CTRL) and the PCM-enhanced mortars (P10-20, P25-20, and P10/25-10), together with the imposed climatic chamber temperature.

For all configurations, the internal hot-box temperature follows the general trend imposed by the climatic chamber; however, clear differences are observed between the PCM-free and PCM-bearing systems. In the reference configuration, temperature variations closely track the external thermal cycle, resulting in pronounced internal temperature peaks and troughs. In contrast, all PCM-enhanced mortars exhibit attenuated temperature oscillations, particularly during the heating phases, indicating an increase in thermal inertia.

Among the PCM-bearing formulations, P25-20 displays the most pronounced reduction in internal temperature fluctuations over successive heating–cooling cycles Fig. 12a). Compared to the reference system, this formulation consistently shows lower peak temperatures and smoother thermal transitions, particularly in the vicinity of the maximum temperature range. This behaviour suggests more effective activation of latent heat storage mechanisms, as the phase-change temperature of PCM25 closely overlaps with the temperature interval repeatedly reached inside the hot-box during the imposed cycles.

The P10-20 formulation also demonstrates a measurable thermal buffering effect, with reduced temperature peaks and a smoother cooling response compared to CTRL (Fig. 12b). However, the attenuation of temperature oscillations is less pronounced than that observed for P25-20. This difference can be attributed to the lower phase-change temperature of PCM10, which is activated primarily during the lower portion of the thermal cycle and therefore contributes less effectively to peak temperature mitigation under the applied heating regime.

The hybrid formulation P10/25-10 exhibits intermediate behaviour between the two single-PCM systems (Fig. 12c). The internal temperature profiles indicate moderate peak attenuation and a slight delay in

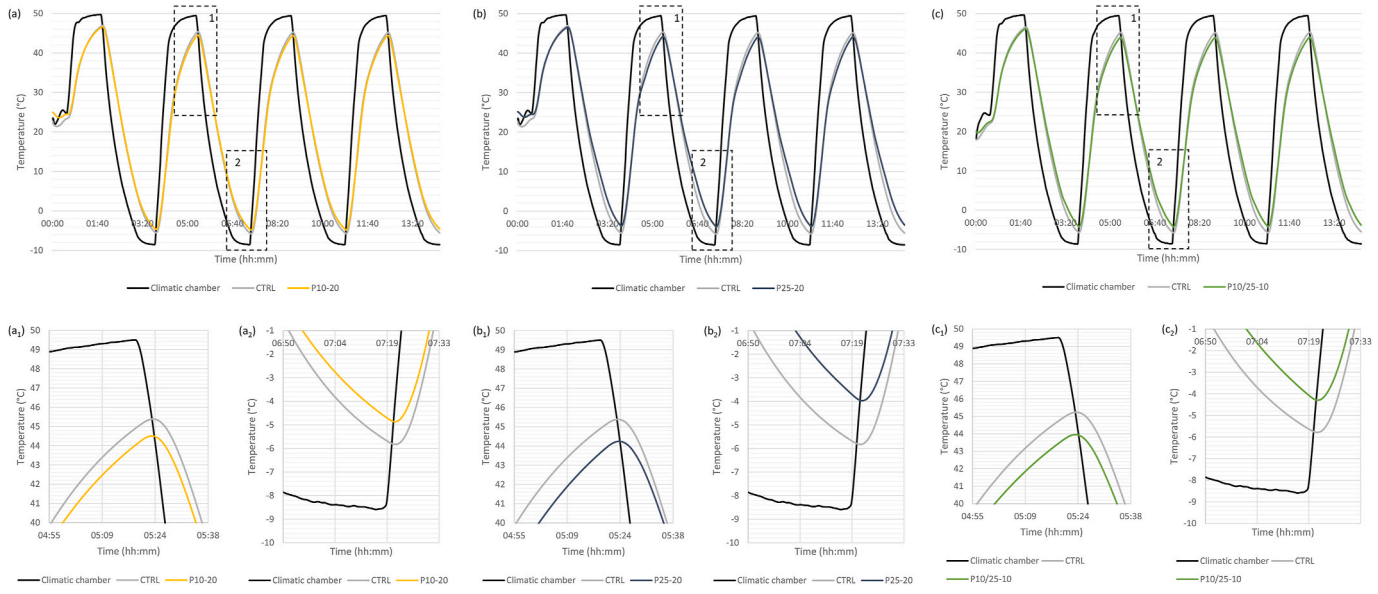


**Fig. 12.** Comparison of internal hot-box temperature profiles under cyclic thermal conditions for (a) CTRL and P10-20, (b) CTRL and P25-20, and (c) CTRL and P10/25-10, together with the imposed climatic chamber temperature. Insets ($a_1$-$a_2$), ($b_1$-$b_2$), and ($c_1$-$c_2$) show magnified views of selected time intervals, highlighting differences in temperature evolution between the reference and PCM-enhanced mortars during representative heating and cooling phases.

temperature evolution during both heating and cooling phases, reflecting the combined contribution of the two PCM types. While the buffering effect is broader in temperature range, its intensity remains lower than that of the P25-20 formulation.

Overall, the hot-box results demonstrate that the effectiveness of PCM-enhanced mortars in regulating temperature under dynamic conditions strongly depends on the alignment between PCM phase-change temperature and the operating thermal range. In the present experimental setup, the P25-20 formulation provides the most effective thermal buffering, followed by the hybrid P10/25-10 and the P10-20 mortar. Rather than altering steady-state temperatures, the PCMs primarily act by reducing the amplitude of temperature fluctuations and increasing thermal inertia, resulting in smoother and more stable internal temperature profiles.

These findings are consistent with the thermal conductivity results, which showed reduced conductivity for PCM-containing mortars, and with the microstructural analyses, which confirmed that PCM incorporation at the investigated dosages does not compromise matrix integrity. From an application perspective, the observed attenuation of temperature peaks and delayed thermal response highlight the potential of PCM-enhanced lime-based mortars, particularly those incorporating PCM25, for façade retrofitting strategies aimed at improving thermal comfort under cyclic thermal loads.

Table 6 summarizes the peak-to-peak temperature amplitudes obtained from the hot-box experiments for the reference and PCM-enhanced mortars, together with the corresponding oscillation reductions relative to the control.

The temperature fluctuation amplitude (ΔT) recorded during the hotbox thermal cycling tests clearly highlights the beneficial effect of PCM incorporation on the thermal buffering capacity of the lime-based mortars. The reference mortar (CTRL) exhibited the highest temperature swing, with a ΔT of 51.44 °C, closely following the external climatic chamber profile. In contrast, all PCM-modified mortars showed reduced temperature amplitudes, indicating an enhanced ability to attenuate thermal extremes through latent heat storage and release.

Among the PCM-bearing formulations, P25-20 exhibited the most pronounced thermal buffering, showing the lowest ΔT value (48.71 °C), which corresponds to an absolute reduction of 2.72 °C and a relative decrease of 5.29% compared to the control. This improved performance can be directly related to the higher heat storage capacity of PCM25, as reported by the manufacturer (150-170 J $g^{-1}$ for dried microcapsules), compared to PCM10 (>110 J $g^{-1}$). The greater latent heat content of PCM25 allows more thermal energy to be absorbed during the heating phase and subsequently released during cooling, resulting in more effective attenuation of temperature peaks and troughs.

The hybrid formulation P10/25-10 also showed a notable reduction in temperature amplitude (ΔT = 48.78 °C; 5.00% reduction), indicating that combining PCMs with different latent heat capacities can also contribute to thermal regulation. However, the slightly higher ΔT compared to P25-20 suggests that the overall thermal response is strongly influenced by the total latent heat storage potential of the incorporated PCM. The P10-20 mortar, containing PCM with lower heat storage capacity, exhibited a more modest yet still significant reduction in temperature fluctuations (ΔT = 49.82 °C; 3.15%).

Despite differences in PCM type and formulation strategy, all PCM-modified mortars displayed stable and repeatable thermal responses across consecutive cycles, confirming the robustness of the thermal storage mechanism. Overall, these results indicate that P25-20 provides the most effective reduction of temperature fluctuations, highlighting the importance of PCM latent heat capacity in optimizing the thermal performance of lime-based mortars for passive thermal regulation, improved thermal comfort and energy-efficient building applications.

**Table 6**
Average peak-to-peak temperature oscillation (ΔT), absolute temperature attenuation relative to the reference mortar ($\Delta T_{red}$), and corresponding relative reduction (%) derived from hot-box experiments.

| Batch | ΔT (°C) | $\Delta T_{red}$ (°C) | Relative reduction (%) |
|---|---|---|---|
| CTRL | 51.44 | - | - |
| P10-20 | 49.82 | 1.62 | 3.15 |
| P25-20 | 48.71 | 2.72 | 5.29 |
| P10/25-10 | 48.78 | 2.57 | 5.00 |

### 3.2. *Durability of the mortars: assessment through accelerated ageing tests*

Durability is a critical parameter for the long-term performance of rendering mortars, as it directly influences service life, maintenance requirements, and overall environmental impact (Belfiore et al., 2023; Branco et al., 2021). In this context, freeze-thaw cycling and salt crystallization tests were employed to assess the resistance of the reference and PCM-modified lime-based mortars to aggressive environmental actions.

The freeze-thaw test revealed clear differences in durability between the reference mortar (CTRL) and the PCM-containing formulations (Fig. 13). The CTRL mortar maintained a relatively stable mass variation during the initial and intermediate cycles, indicating limited surface damage at early stages. However, a pronounced mass loss occurred during the final cycles, reflecting the onset of severe deterioration and loss of material integrity before completion of the test. This behaviour is corroborated by the visual assessment of the specimens (Fig. 14), where the CTRL mortar exhibits clear signs of surface degradation and material loss by the end of the testing sequence. This delayed but abrupt degradation pattern is characteristic of lime-based mortars subjected to repeated freeze-thaw action, where cumulative damage progressively weakens the microstructure until critical failure is reached. The observed behaviour is consistent with the known susceptibility of lime mortars to freeze-thaw stress under conditions of repeated moisture ingress and temperature cycling. In contrast, all PCM-modified mortars demonstrated substantially improved resistance to freeze-thaw action. The formulations P10-20, P25-20, and P10/25-10 maintained a relatively stable mass variation throughout the test cycles, indicating no surface scaling and delayed damage progression.

Similar trends were observed in the salt crystallization test (Fig. 15), which represents one of the most aggressive degradation mechanisms for lime-based materials. The CTRL mortar experienced rapid mass loss, even from the 4th cycle, indicative of severe surface scaling and progressive disintegration caused by repeated salt crystallization pressures within the pore network. Failure occurred at an early stage, confirming the limited resistance of the reference formulation to saline environments.

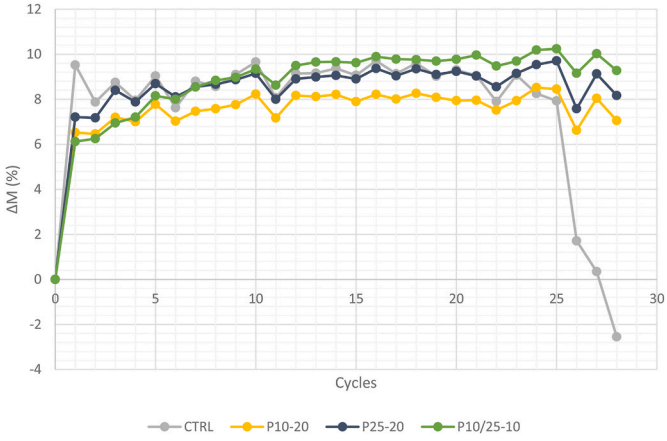


**Fig. 13.** Mass variation (ΔM, %) of lime-based mortars during the freeze-thaw test, as a function of the number of cycles, comparing the reference mortar (CTRL) with PCM-containing mortars (P10-20, P25-20, and P10/25-10).

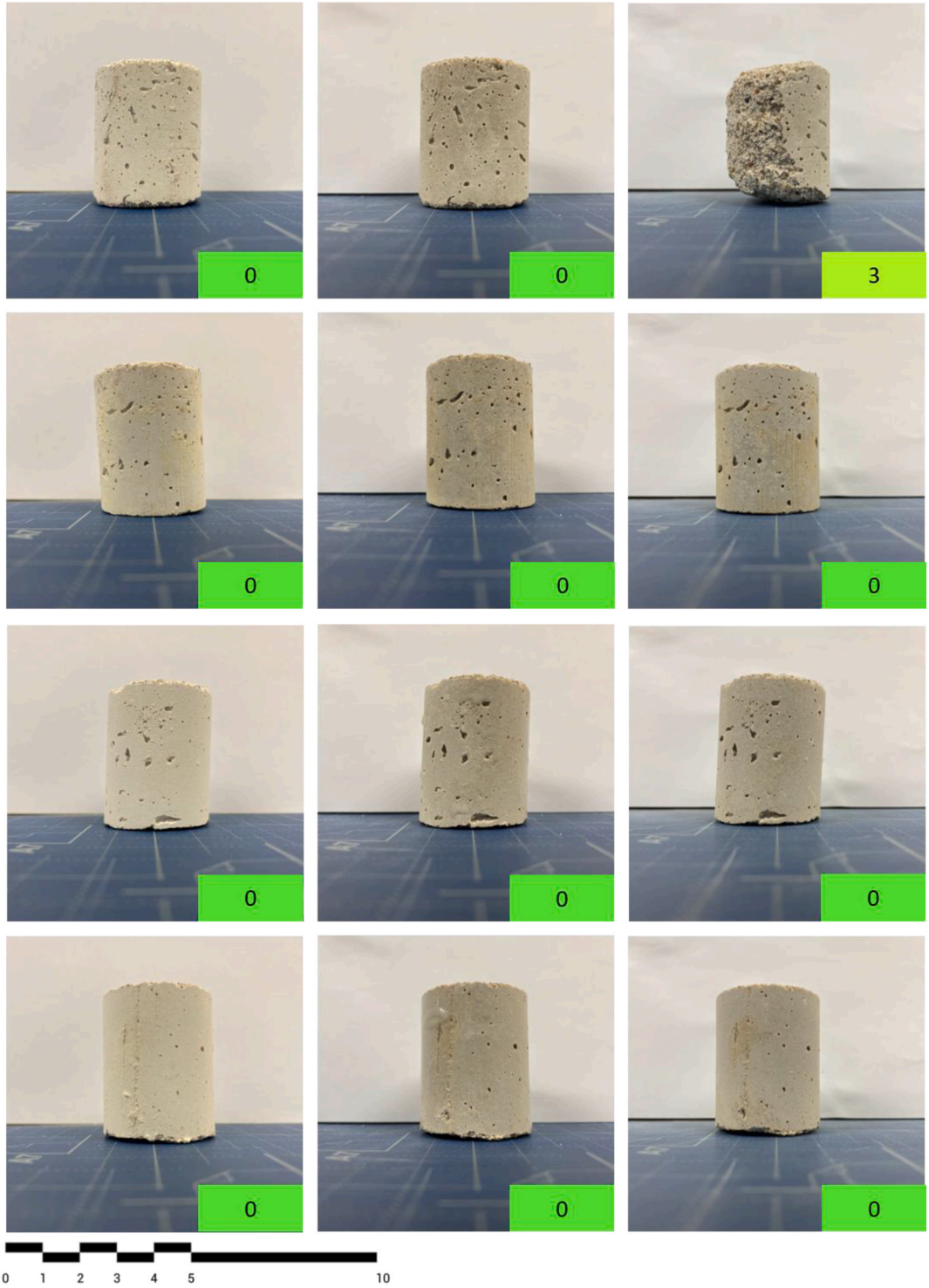


**Fig. 14.** Visual assessment of mortar specimens subjected to freeze–thaw cycles. Rows correspond to CTRL, P10-20, P25-20, and P10/25-10 mortars (top to bottom), while columns show the specimens before testing, after 14 cycles, and after 28 cycles (left to right). Each individual sample shown is representative of the average state of all samples tested. Coloured markers indicate the damage classification level defined in Table 3. Scale bar in centimeters.

Conversely, all PCM-containing mortars exhibited markedly improved performance, successfully withstanding a significantly higher number of cycles with comparatively lower mass loss. The mass variation curves of P10-20, P25-20, and P10/25-10 suggest a more gradual deterioration process, characterized by moderate surface damage rather than catastrophic failure. A comparable improvement in salt crystallization resistance for PCM-modified lime-based mortars has also been reported by Theodoridou et al. (2026), who attributed this behaviour to modifications in pore structure and moisture transport induced by PCM incorporation, supporting the trends observed in the present study.

These quantitative trends are fully supported by the visual assessment of the specimens (Fig. 16). The CTRL mortar exhibited extensive surface scaling, material detachment, and pronounced loss of cohesion by the early stages of the test, in agreement with the rapid mass loss recorded. In contrast, the PCM-modified mortars showed substantially milder surface deterioration, with damage largely confined to

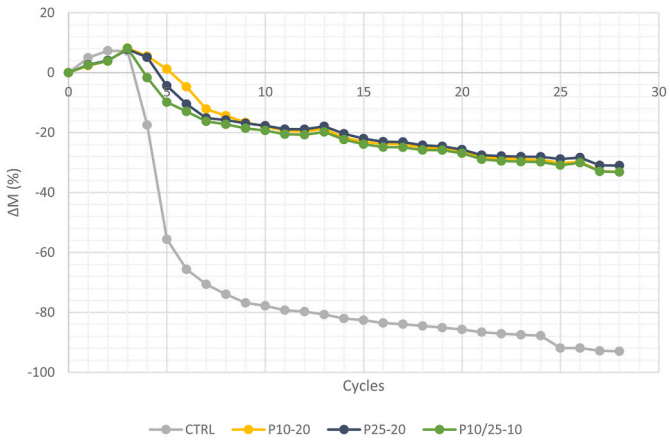


**Fig. 15.** Mass variation (ΔM, %) of lime-based mortars during the salt crystallization test, as a function of the number of cycles, for the reference mortar (CTRL) and PCM-modified formulations (P10-20, P25-20, and P10/25-10).

superficial areas and no evidence of structural collapse. The good agreement between mass variation data and qualitative observations confirms that PCM incorporation effectively mitigates salt crystallization-induced damage, enhancing the resistance of lime-based mortars to aggressive saline environments.

The improved resistance to freeze-thaw and salt crystallization in PCM-modified mortars may be attributed to modifications in the pore network and moisture transport pathways induced by PCM incorporation. Changes in pore size distribution and capillary connectivity can influence water or salt solution ingress and crystallization dynamics, potentially reducing crystallization pressures acting on the matrix. Although PCM addition may increase total porosity, the disruption of continuous capillary pathways appears to play a beneficial role in limiting damage severity.

It should be noted that the applied freeze-thaw and salt crystallization tests are accelerated laboratory procedures designed to simulate key degradation mechanisms affecting mortars in historic masonry, particularly in environments exposed to moisture and soluble salts. While these tests provide valuable and reproducible information on the relative resistance of different formulations, they do not fully reproduce the complexity of real environmental conditions, where multiple factors such as temperature fluctuations, relative humidity, solar radiation, and wetting-drying cycles interact over extended periods. Therefore, the results should be interpreted as indicative of the material's resistance to specific deterioration processes rather than as a direct prediction of long-term in-situ performance. In this context, the combined use of laboratory durability testing and field-scale monitoring in the present study provides a more comprehensive assessment of material behaviour under both controlled and real exposure conditions.

### *3.3. Multi-criteria performance evaluation of ternary mortars using a modified property method*

The outcomes of the modified weighting property analysis are presented in Fig. 17a–b, which includes a radar plot illustrating the normalized contribution of individual properties and a bar chart summarizing the total performance index for each mix design.

The radar plot (Fig. 17a) highlights clear differences in the performance profiles of the investigated mortars under the defined weighting scenario for external thermal renders. As expected from the assigned importance factors, thermally driven parameters, namely latent heat storage, thermal conductivity, and hot-box performance, dominate the overall performance envelope. The PCM-enhanced formulations clearly expand along the latent heat storage axis, particularly P10/25-10 and P25-20, reflecting their superior energy storage capacity compared to the reference mortar. The hot-box parameter (ΔT) appears comparable across all PCM formulations and remains one of the strongest contributors to the total index.

In contrast, the reference mortar (CTRL) exhibits negligible contribution in latent heat storage, as anticipated due to the absence of PCM, and therefore lacks one of the most heavily weighted performance drivers in the present scenario. Although CTRL shows acceptable compressive strength, this criterion was intentionally assigned lower relative importance within the weighting framework. For rendering mortars applied as non-structural external layers, compressive strength beyond a minimum threshold is generally not the governing design parameter, provided that mechanical integrity and adhesion are sufficient to ensure service performance. Consequently, the overall performance envelope of CTRL is reduced primarily because it cannot compete in the thermally weighted dimensions, which are central to the intended retrofit application.

Among the PCM-containing mortars, P10/25-10 presents the most extended radial distribution in the thermally weighted criteria while maintaining competitive durability performance. P25-20 exhibits a relatively balanced profile across thermal conductivity, freeze-thaw resistance, and salt crystallization resistance. P10-20, although thermally improved compared to CTRL, shows a more moderate expansion in latent heat storage and a slightly narrower global envelope. Overall, the radar diagram confirms that the ranking is primarily driven by thermal functionality, as intended by the selected weighting scenario.

The bar chart of the total performance index (Fig. 17b) provides a direct and quantitative ranking of the investigated formulations. The reference mortar (CTRL) exhibits the lowest overall index, reflecting its lack of latent heat storage and its limited contribution to the thermally weighted criteria. In contrast, all PCM-enhanced formulations achieve substantially higher indices, clearly demonstrating the impact of PCM incorporation under the selected application scenario.

Among them, P25-20 and P10/25-10 present the highest total performance indices, followed by P10-20. The relatively small difference between P25-20 and the hybrid P10/25-10 indicates that both formulations provide strong thermally driven performance while maintaining satisfactory durability-related properties. Their higher ranking is primarily governed by superior latent heat storage capacity and improved hot-box performance, which were assigned the highest weighting factors in the present evaluation framework.

Durability-related parameters (freeze-thaw resistance and salt crystallization resistance) also contribute significantly to the global index, reflecting their importance from both a technical and sustainability perspective. Enhanced durability reduces the frequency of maintenance interventions, material replacement, and associated embodied carbon impacts over the service life of the building envelope. In this sense, durability is not only a performance requirement but also a key component of low-carbon and conservation-oriented retrofit strategies.

Although compressive strength values are comparable, and in some cases slightly higher, for PCM-modified mortars relative to CTRL, this property exerts only a limited influence on the overall ranking due to its intentionally low weighting within the defined application scenario. Consequently, the global performance index is primarily controlled by thermophysical and durability-related parameters rather than by mechanical strength.

Overall, the multi-criteria assessment confirms that, when thermal enhancement is defined as the primary design objective, PCM incorporation leads to a clear and quantifiable improvement in global performance. The adopted weighting methodology thus provides a transparent framework linking laboratory-derived properties with application-specific priorities, supporting rational mix-design selection for thermally enhanced external renders while integrating both energy efficiency and long-term durability considerations.

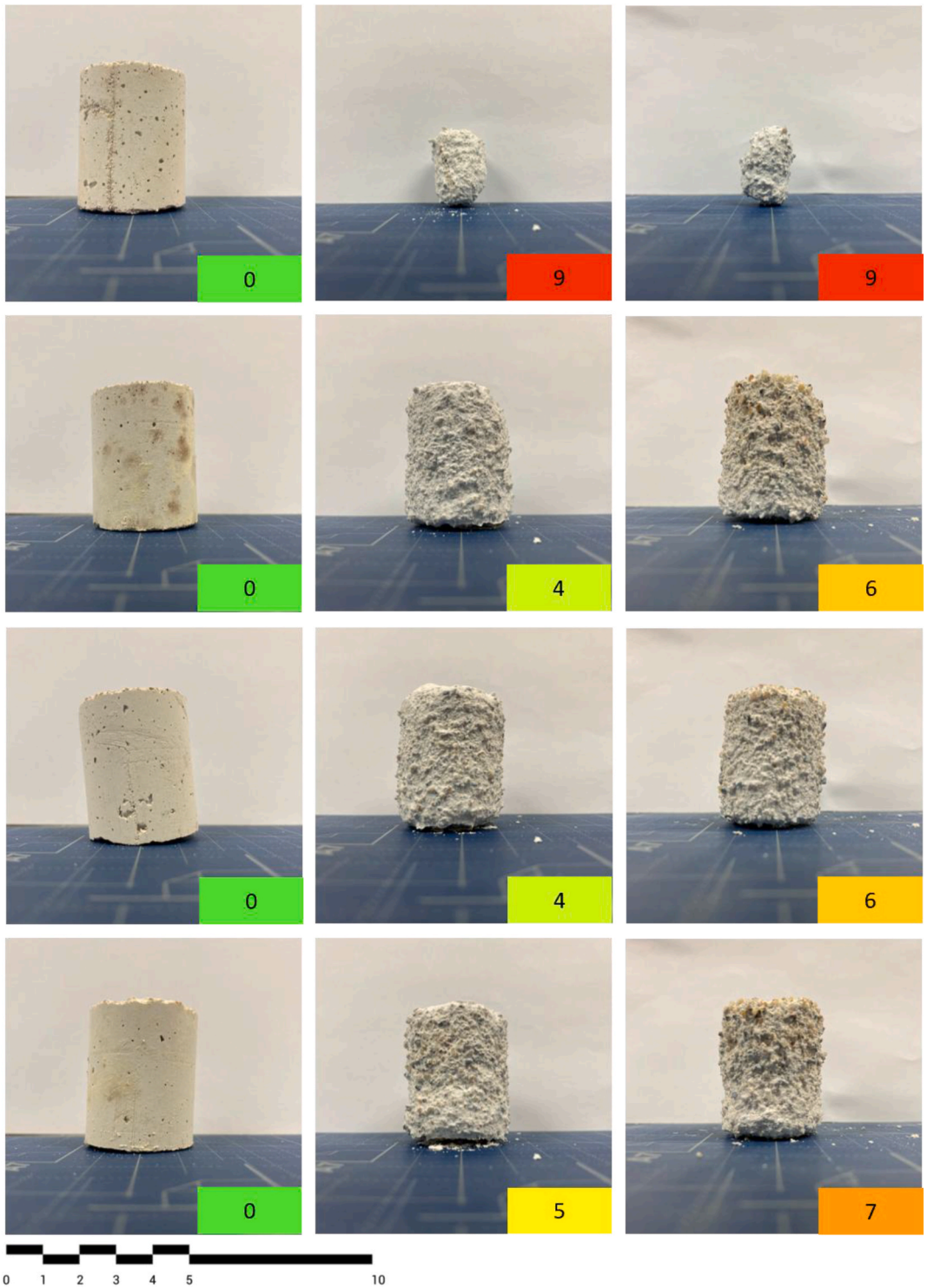


**Fig. 16.** Visual assessment of mortar specimens subjected to salt crystallization cycles. Rows correspond to CTRL, P10-20, P25-20, and P10/25-10 mortars (top to bottom), while columns show the specimens before testing, after 14 cycles, and after 28 cycles (left to right). Each individual sample shown is representative of the average state of all samples tested. Coloured markers indicate the damage classification level defined in Table 3. Scale bar in centimeters.

## 4. Assessment of the performance under real exposure conditions: pilot site and mock-up results

Fig. 18 presents the monitored thermal response of the east-oriented façades of the reference mock-up (REF) and the PCM-enhanced mock-up (MOC3) during two representative six-day periods: late summer (Fig. 18$a_1$-$a_2$) and early autumn (Fig. 18$b_1$-$b_2$). The datasets include temperatures measured at the exposed mortar surface (E-MU), at the block-mortar interface (E-BU), at the internal wall surface (E-IU), and the corresponding internal heat flux (E-IU-Flux), together with the ambient outdoor air temperature.

In both monitoring periods, the external/exposed mortar temperatures (E-MU) show the strongest coupling with the ambient climatic forcing, exhibiting sharp diurnal peaks and troughs driven by outdoor temperature fluctuations and solar exposure. For both REF and MOC3, the timing and magnitude of these surface temperature variations are

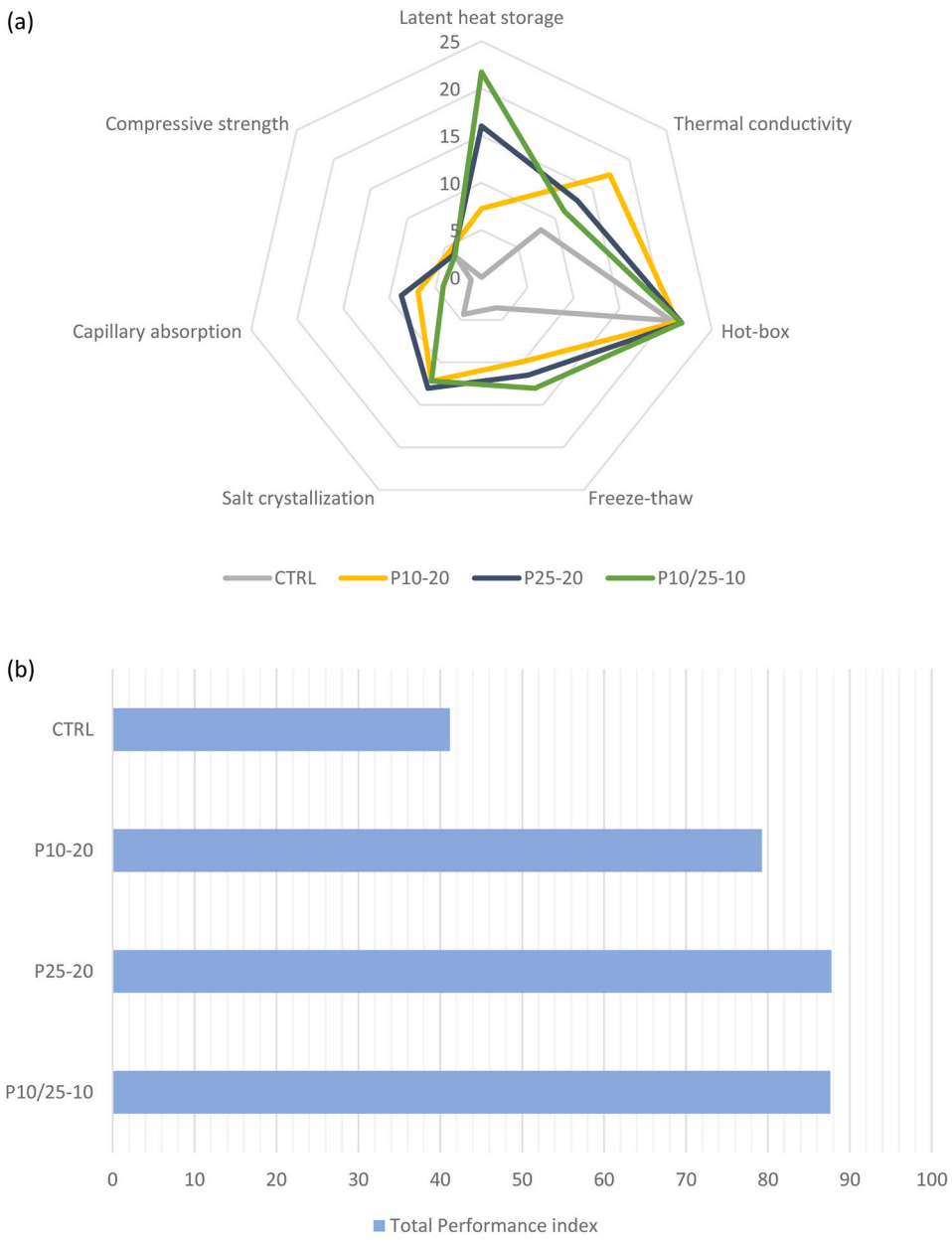


**Fig. 17.** Multi-criteria performance evaluation of the investigated mortar formulations for external rendering applications with thermal enhancement: (a) radar representation of the weighted performance contribution of each property (latent heat storage, thermal conductivity, hot-box performance, freeze-thaw resistance, salt crystallization resistance, capillary absorption, and compressive strength); (b) total performance index (I) derived from the modified weighting property method, enabling direct ranking of the mix designs under the defined application scenario.

largely similar, indicating that the presence of PCMs does not substantially alter the short-term thermal behaviour at the outermost layer of the façade, where boundary conditions dominate heat exchange.

Clearer differences emerge at the internal side of the wall assembly. The internal surface temperature (E-IU) of the PCM-enhanced mock-up is systematically higher than that of the reference configuration, with a mean offset of approximately 1-2 °C, throughout both the summer and autumn periods. At the same time, the MOC3 internal temperature signal exhibits smoother diurnal evolution, with reduced day-night temperature swings, typically of 1-3 °C, compared to the reference. This effect is particularly evident during nocturnal and early-morning hours, when the reference façade experiences more pronounced cooling, while the PCM-enhanced façade maintains a higher internal temperature level.

The internal heat-flux measurements (E-IU-Flux) further support this interpretation. For both façades, the heat-flux signals display a clear daily periodicity, with positive excursions associated with daytime heat transfer driven by external warming. However, the PCM-enhanced façade tends to exhibit broader and more temporally distributed flux peaks, rather than sharp, transient maxima. This indicates that thermal energy transfer through the PCM-modified wall occurs over a longer duration, consistent with delayed heat release and increased effective thermal inertia.

The observed behaviour is coherent across both seasonal datasets. During summer, when external temperatures frequently exceed the nominal phase-change temperature of the PCM (25 °C), the PCM-enhanced render moderates rapid temperature changes within the wall, limiting sharp internal temperature fluctuations while sustaining higher internal temperatures during cooler periods. During autumn, when ambient temperatures oscillate closer to the PCM activation range, a similar but more moderate effect is observed, with the PCM façade continuing to exhibit smoother internal temperature profiles and

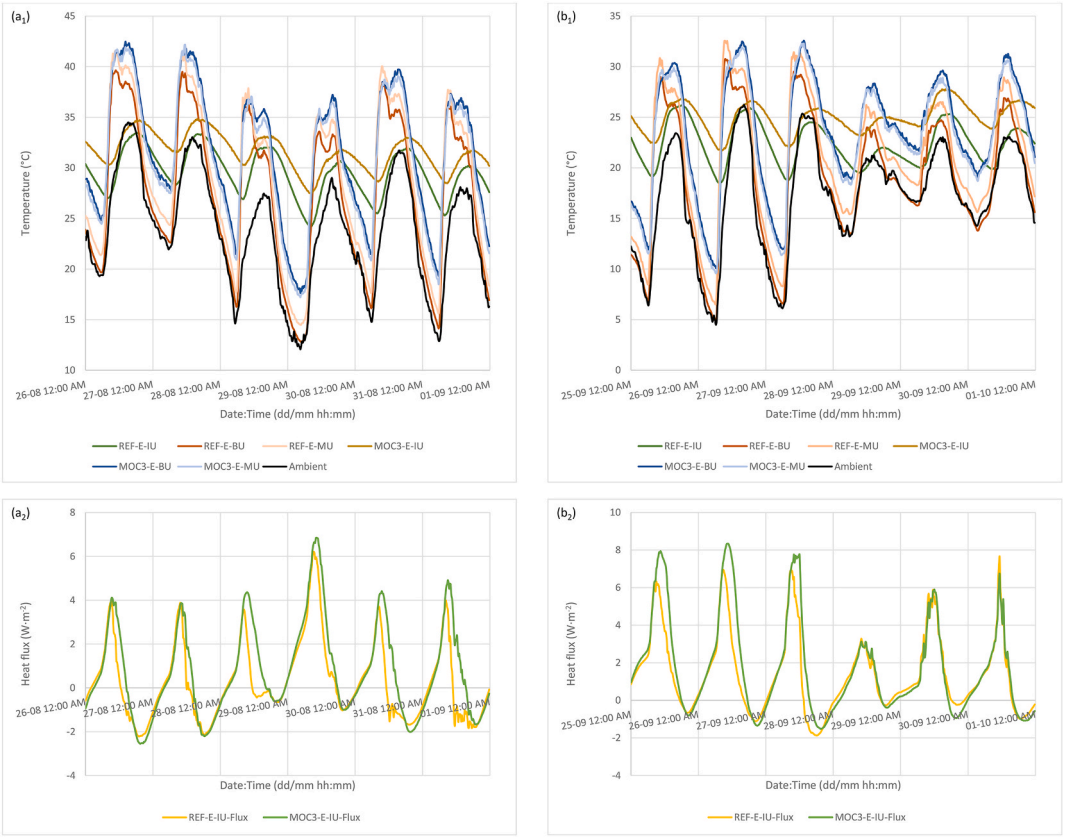


**Fig. 18.** Temperature and heat-flux evolution of the east-facing reference (REF) and PCM-enhanced (MOC3) façades during the monitored periods. (a1) Temperature profiles during summer (26–31 August 2025); (a2) corresponding heat-flux measurements. (b1) Temperature profiles during autumn (25–30 September 2025); (b2) corresponding heat-flux measurements.

redistributed heat-flux patterns relative to the reference.

Overall, the monitoring results demonstrate that the primary impact of PCM incorporation is expressed within the wall assembly and at the internal interface, rather than at the exposed surface. The PCM-enhanced façade does not eliminate heat transfer but modifies its temporal distribution, attenuating short-term thermal extremes and contributing to a more stable internal thermal environment. This behaviour aligns with the intended function of microencapsulated PCMs embedded in rendering mortars, which act as passive thermal buffers by storing and releasing latent heat within temperature ranges relevant to building operation.

The interior air temperature recorded by the THL sensor highlights the influence of PCM incorporation on the thermal conditions within the mock-up enclosure (Fig. 19a and b). The reference configuration exhibits higher air temperature levels and more pronounced diurnal fluctuations, closely following the variations imposed by the external environment. In contrast, Mockup-3, incorporating the PCM-enhanced render, shows systematically lower temperature values and a smoother temporal evolution.

A quantitative summary of the peak-to-peak daily temperature amplitudes over the monitored six-day periods is provided in Table 7. During the summer campaign, the reference configuration exhibited an average interior daily ΔT of 4.20 °C, whereas Mockup-3 showed a reduced average amplitude of 2.61 °C. Similarly, during the autumn period, the reference façade recorded an average ΔT of 4.14 °C compared to 2.57 °C for the PCM-enhanced system. These results correspond to an approximate reduction of 38% in daily interior temperature amplitude for both monitoring periods.

This behaviour indicates that the PCM-modified façade contributes to moderating the indoor air temperature within the enclosure, as reflected by the reduced amplitude and damped daily oscillations measured by the centrally located THL sensor. The attenuation of temperature fluctuations suggests that the presence of microencapsulated PCM limits the intensity of indoor temperature peaks during periods of elevated external temperatures, while promoting a more gradual thermal response over time. This effect is consistent with the latent heat storage and release mechanism of PCMs, which temporarily absorb excess heat during heating phases and release it during cooling, thereby redistributing thermal energy over longer time scales.

As a result, the PCM-enhanced system maintains a more stable interior air temperature compared to the reference façade, indicating an improved capacity to regulate indoor thermal conditions under dynamic boundary conditions.

From a building performance perspective, the observed reduction in indoor temperature fluctuations has direct implications for both energy consumption and thermal comfort. The attenuation of peak temperatures during daytime reduces the risk of overheating, while the moderated nocturnal cooling and delayed heat release contribute to limiting heat losses. As a result, the intensity and frequency of heating and cooling system operation may be reduced, particularly under conditions of pronounced diurnal thermal variability. In addition, the smoother indoor temperature profiles observed in the PCM-enhanced façade contribute to improved thermal comfort by minimizing abrupt temperature swings within the enclosure. Although direct quantification of energy savings is beyond the scope of the present study, the measured reduction in daily temperature amplitude (approximately 38%) provides strong evidence of the potential of PCM-enhanced renders to contribute to reduced energy demand and improved indoor environmental conditions under real operating conditions.

A comparison between the laboratory hot-box results and the field-scale monitoring data reveals both consistent trends and notable differences in the thermal behaviour of the PCM-enhanced mortars. In both

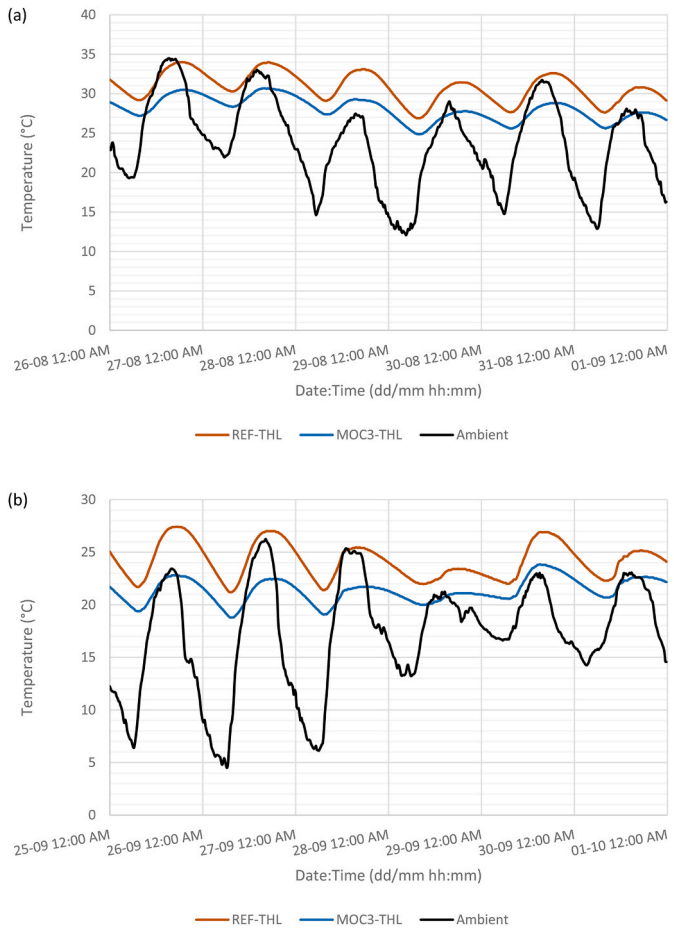


**Fig. 19.** Evolution of the interior air temperature measured by the THL sensor for the reference façade (REF) and the PCM-enhanced façade (Mockup-3) under real outdoor conditions at the Algete pilot site during representative monitoring periods: (a) 26-31 August 2025 (summer, 6 days) and (b) 25-30 September 2025 (autumn, 6 days). The corresponding ambient air temperature is included for reference.

**Table 7**
Average peak-to-peak temperature oscillation measured in summer and autumn for the reference (REF) and PCM-enhanced mock-up (MOC3).

| Mock-up | $\Delta T_{summer}$ (°C) | $\Delta T_{autumn}$ (°C) |
|---|---|---|
| REF | 4.20 | 4.14 |
| MOC3 | 2.61 | 2.57 |

cases, the incorporation of PCM leads to attenuation of temperature fluctuations and a smoothing of the thermal response, confirming the effectiveness of latent heat storage under dynamic thermal loading. However, the magnitude of the effect observed in the field-scale mock-ups differs from that measured in the controlled hot-box experiments. While the hot-box tests are characterized by well-defined and repeatable thermal cycles, the field results are influenced by complex and variable boundary conditions, including solar radiation, ambient temperature fluctuations, and heat transfer through the full wall assembly. As a result, the thermal buffering effect in the field is more gradual and distributed over time, rather than sharply defined as in the laboratory tests.

Despite these differences, the overall agreement between laboratory and field observations supports the validity of the experimental approach and confirms that the thermal performance trends identified under controlled conditions are representative of real operating behaviour. This consistency strengthens the applicability of PCM-enhanced mortars for façade retrofitting under realistic environmental conditions.

## 5. Implications, limitations and future perspectives

The findings of this study demonstrate that the integration of microencapsulated phase change materials into ternary lime-pozzolan-cement mortars represents a viable strategy for enhancing the thermal performance of rendering systems within conservation-oriented retrofit frameworks. The experimental campaign confirms that thermal functionality can be introduced without compromising the essential requirements of mechanical compatibility and durability, which are fundamental in heritage applications.

From a design perspective, the study highlights that PCM-enhanced mortars should not be evaluated solely on the basis of peak thermal attenuation or latent heat capacity. Rather, optimal performance emerges from the balanced interaction between thermophysical behaviour, microstructural stability, and durability under environmental stressors. The multi-criteria assessment approach adopted herein reinforces this concept, demonstrating that rational material selection must account for application-specific priorities rather than isolated material properties.

The investigation of hybrid PCM systems further suggests that combining phase change materials with different transition temperatures can broaden the operational thermal window of rendering mortars. Such an approach provides flexibility in tailoring the thermal response to varying climatic contexts, including regions characterized by pronounced seasonal or diurnal fluctuations. This design strategy may be particularly relevant in conservation practice, where interventions must remain reversible, compatible, and minimally invasive while still addressing contemporary energy-efficiency demands.

Field-scale monitoring at the Algete pilot site confirms that laboratory-scale observations translate into measurable in-situ performance. The moderation of internal temperature fluctuations under real environmental exposure demonstrates the practical feasibility of PCM-enhanced renders as passive thermal regulators within façade assemblies. These findings strengthen the technological readiness of such materials for implementation in both traditional masonry heritage and twentieth-century reinforced concrete architecture.

Nevertheless, certain aspects merit further exploration. Although the present study provides robust laboratory and field-scale validation, extended monitoring under prolonged thermal cycling and aging conditions would further consolidate the long-term reliability of PCM-enhanced lime-based renders. Ongoing investigations are currently addressing these aspects to better understand the durability of the latent heat mechanism under repeated environmental loading.

In addition, while previous work has examined the carbon footprint and climate-dependent energy performance of PCM-lime mortars (Rubio-Aguinaga et al., 2025a), broader life-cycle assessments incorporating service-life extension, maintenance frequency, and whole-envelope performance would provide a more comprehensive evaluation of their sustainability potential. Such analyses are particularly relevant in conservation contexts, where durability and reduced intervention frequency directly influence embodied carbon and resource consumption over time.

Future research should therefore focus on integrating long-term durability assessment, climatic optimization of PCM transition temperatures, and coupled hygrothermal-energy modelling approaches. Expanding validation to full-scale building case studies and exploring synergies with other passive retrofit strategies may further advance the development of multifunctional, conservation-compatible, and low-carbon rendering systems for heritage and modern building envelopes.

## 6. Conclusions

This study evaluated the performance of ternary lime-pozzolan-

cement mortars incorporating microencapsulated phase change materials for conservation-oriented thermal retrofitting. Based on laboratory characterization, durability assessment, multi-criteria ranking, and field validation, the following conclusions can be drawn:

- Thermal conductivity of PCM-enhanced mortars was significantly reduced compared to the reference formulation, with values decreasing from approximately 0.63-0.65 W $m^{-1}{\cdot}K^{-1}$ to a range of 0.30-0.48 W $m^{-1}{\cdot}K^{-1}$ at 182 days of curing.
- Differential scanning calorimetry confirmed persistent latent heat storage within the hardened matrix, with melting enthalpies of approximately 0.8 J $g^{-1}$ (P10-20), 1.9 J $g^{-1}$ (P25-20), and up to 2.7 J $g^{-1}$ for the hybrid P10/25-10 formulation.
- Hot-box testing demonstrated measurable attenuation of internal temperature oscillations under cyclic loading. The reference mortar exhibited an average peak-to-peak temperature amplitude of 51.44 °C, while PCM incorporation reduced this to 49.82 °C (P10-20), 48.71 °C (P25-20), and 48.78 °C (P10/25-10), corresponding to relative reductions of 3.15%, 5.29%, and 5.00%, respectively. The P25-20 formulation achieved the highest peak attenuation.
- Microstructural analysis confirmed stable embedding and preservation of PCM microcapsules within the binder matrix, without evidence of structural disruption.
- Durability testing under freeze-thaw and salt crystallization cycles showed performance comparable to or superior to the reference mortar, indicating that PCM incorporation does not compromise environmental resistance when properly formulated.
- The multi-criteria performance index identified P25-20 and P10/25-10 as the most suitable formulations for thermally enhanced external rendering applications, reflecting their balanced thermophysical efficiency and durability performance.
- Field-scale monitoring at the Algete pilot site validated laboratory findings. During representative 6-day monitoring periods, the average interior air peak-to-peak temperature amplitude decreased from 4.20 °C to 2.61 °C in summer and from 4.14 °C to 2.57 °C in autumn when comparing the reference façade to the PCM-enhanced façade, confirming consistent moderation of diurnal thermal fluctuations under real outdoor exposure.

Overall, PCM-enhanced ternary lime-based mortars provide effective passive thermal regulation while maintaining mechanical compatibility and durability requirements for conservation applications. The incorporation of mixed PCM systems represents a promising pathway for tailoring thermal performance to specific climatic conditions, supporting the development of multifunctional and conservation-compatible retrofit materials.

## CRediT authorship contribution statement

**Loucas Kyriakou:** Conceptualization, Data curation, Formal analysis, Investigation, Methodology, Validation, Visualization, Writing – original draft. **Andrea Rubio-Aguinaga:** Data curation, Investigation, Methodology, Visualization, Writing – original draft. **Mohammad Hossein Nofalah:** Data curation. **Laura Maria Piarulli Paz:** Data curation, Methodology, Visualization, Writing – review & editing. **Álvaro García Molino:** Data curation, Methodology. **Liberato Ferrara:** Project administration, Writing – review & editing. **Ioannis Karatasios:** Funding acquisition, Project administration, Resources, Writing – review & editing. **Eirini Tziviloglou:** Project administration, Writing – review & editing. **José María Fernández:** Conceptualization, Formal analysis, Resources, Writing – review & editing. **Íñigo Navarro-Blasco:** Conceptualization, Formal analysis, Funding acquisition, Resources, Supervision, Validation. **José Ignacio Álvarez:** Conceptualization, Formal analysis, Funding acquisition, Project administration, Resources, Supervision, Validation, Writing – review & editing.

## Declaration of competing interest

The authors declare that they have no known competing financial interests or personal relationships that could have appeared to influence the work reported in this paper.

## Acknowledgements

The authors express their gratitude for the technical support provided by Cristina Luzuriaga.

This work was co-funded by the European Union's Horizon Europe research and innovation programme, under Grant Agreement No 101123293 (SINCERE - The Second Life of Modern Period Architecture: Resilient and Adaptive Renovation towards Net-Zero Carbon Heritage Buildings) and by Gobierno de España, Ministerio de Ciencia e Innovación, MICINN/AEI/10.13039/501100011033, grant PID2020-119975RB-I00, LIMORTHER.

## Data availability

The data that has been used is confidential.

## References

Akeiber, H., Nejat, P., Majid, M., Wahid, M.A., Jomehzadeh, F., Famileh, I.Z., Calautit, J. K., Hughes, B.R., Zaki, S.A., 2016. A review on phase change material (PCM) for sustainable passive cooling in building envelopes. Renew. Sustain. Energy Rev. 60, 1470–1497.

Andrejkovičová, S., Maljaee, H., Rocha, D., Rocha, F., Soares, M.R., Velosa, A., 2022. Mortars for conservation of late 19th and early 20th century buildings—combination of natural cements with air lime. Materials 15 (10), 3704.

Asadi, E., Gameiro da Silva, M., Antunes, C.H., Dias, L., 2012. Multi-objective optimization for building retrofit strategies: a model and an application. Energy Build. 44, 81–87.

Asadi, I., Baghban, M.H., Hashemi, M., Izadyar, N., Sajadi, B., 2022. Phase change materials incorporated into geopolymer concrete for enhancing energy efficiency and sustainability of buildings: a review. Case Stud. Constr. Mater. 17, e01162.

Šavija, B., 2018. Smart crack control in concrete through use of phase change materials (PCMs): a review. Materials 11 (5), 654.

Baccega, E., Bottarelli, M., 2022. Granular PCM-enhanced plaster for historical buildings: experimental tests and numerical studies. Energies 15 (3), 975.

Baccega, E., Bottarelli, M., 2025. Lime-plaster enhanced with phase-change materials: an experimental monitoring analysis. Green Technol. Innovat. 1 (1), 8108.

Barbosa, M., Innocencio, C.d.R., Salzani, L.O., Pereira, T.d.S., Dias de Souza, N.G., Cappa de Oliveira, L., 2023. Lime-based mortars with added silica fume and bioproducts for restoration and preservation of heritage buildings. J. Build. Pathol. Rehabil. 8 (37).

Belfiore, C., Montalto, G., Finocchiaro, C., Cultrone, G., Mazzoleni, P., 2023. Durability tests on lime-based mortars from the historic built heritage of catania (Eastern Sicily, Italy): an experimental study. J. Build. Eng. 80, 108137.

Biswas, K., Lu, J., Soroushian, P., Shrestha, S., 2014. Combined experimental and numerical evaluation of a prototype nano-PCM enhanced wallboard. Appl. Energy 131, 517–529.

Blumberga, A., Freimanis, R., Biseniece, E., Kamenders, A., 2023. Hygrothermal performance evaluation of internally insulated historic stone building in a cold climate. Energies 16 (2), 866.

Bose, P., Amirtham, V.A., 2016. A review on thermal conductivity enhancement of paraffinwax as latent heat energy storage material. Renew. Sustain. Energy Rev. 65, 81–100.

Branco, F.G., Belgas, M., Mendes, C., Pereira, L., Ortega, J., 2021. Characterization of fresh and durability properties of different lime mortars for being used as masonry coatings in the restoration of ancient constructions. Sustainability 13 (9), 4909.

Building lime - part 1: definitions, specifications and conformity criteria, EN 459-1," European Committee for Standarization, 2011.

Cement - Part 1: Composition, Specifications and Conformity Criteria for Common Cements, EN 197-1, 2011. European Committee for Standardization.

Coppola, L., Coffetti, D., Lorenzi, S., 2016. Cement-based renders manufactured with phase-change materials: applications and feasibility. Adv. Mater. Sci. Eng. 2016 (1), 7254823.

Dimou, A., Metaxa, Z.S., Kourkoulis, S.K., Karatasios, I., Alexopoulos, N.D., 2022. Tailoring the binder matrix of lime-based binders for restoration interventions with regard to mechanical compatibility. Constr. Build. Mater. 315, 125717.

Drissi, S., Ling, T., Mo, K., Eddhahak, A., 2019. A review of microencapsulated and composite phase change materials: alteration of strength and thermal properties of cement-based materials. Renew. Sustain. Energy Rev. 110, 467–484.

Ferencz, M., Nemeth, B., Gyenis, J., Feczko, T., 2025. Statistical evaluation of PCM plaster lining impact on indoor temperature fluctuation due to variability of outdoor temperature and solar radiation along a whole spring season. J. Build. Eng. 99, 111626.

Frahat, N.B., Amin, M., Heniegal, A.M., Ibrahim, O.O., 2023. Optimizing microencapsulated PCM ratios of sustainable cement mortar for energy savings in buildings. Constr. Build. Mater. 391, 131844.
Frigione, M., Lettieri, M., Sarcinella, A., 2019. Phase change materials for energy efficiency in buildings and their use in mortars. Materials 12 (8), 1260.
Gao, M., Zhao, S., Yang, H., Wu, X., Xiao, Y., 2024. An analysis of the influence of DSC parameters on the measurement of the thermal properties of phase-change material. Materials 17 (23), 5689.
Groot, C., Veiga, R., Papayianni, I., Van Hees, R., Secco, M., Álvarez, J., Faria, P., Stefanidou, M., 2022. RILEM TC 277-LHS report: lime-based mortars for restoration–a review on long-term durability aspects and experience from practice. Mater. Struct. 55, 245.
Hall, C., Hoff, W.D., 2002. Water Transport in Brick, Stone and Concrete, third ed. Taylor & Francis Group, London.
Hattan, H.A., Madhkhan, M., Marani, A., 2021. Thermal and mechanical properties of building external walls plastered with cement mortar incorporating shape-stabilized phase change materials (SSPCMs). Constr. Build. Mater. 270, 121385.
Illampas, R., Rigopoulos, I., Ioannou, I., 2021. Influence of microencapsulated Phase Change Materials (PCMs) on the properties of polymer modified cementitious repair mortar. J. Build. Eng. 40, 102328.
Kadhim, J., Al-Bassam, M., Abdas, S., 2011. Materials selection in conceptual design using weighting property method. Eng. Technol. J. 29, 82–95.
Kaur, G., Fernández, J., Navarro-Blasco, Í., Pavia, S., Álvarez, J., 2026. Photoreactive red mud cementitious composites for environmental remediation. Clean. Eng. Technol. 30, 101153.
Kumar, D.N., Kumar, P.R., 2022. Investigations on alternate lime-pozzolana based mortars for repair of heritage structures. Constr. Build. Mater. 341, 127776.
Li, G., Xu, G., Zhang, J., 2024. Experimental investigation of thermal and mechanical characteristics of slag cement mortars with PCM for radiant floors. Case Stud. Constr. Mater. 20, e02958.
Liu, H., Wang, X., Wu, D., 2019. Innovative design of microencapsulated phase change materials for thermal energy storage and versatile applications: a review. Sustain. Energy Fuels 3, 1091–1149.
Marcos, I., San-José, J., Garmendia, L., Santamaría, A., Manso, J., 2016. Central lessons from the historical analysis of 24 reinforced-concrete structures in northern Spain. J. Cult. Herit. 20, 649–659.
Martín-Garín, A., Millán-García, J., Terés-Zubiaga, J., Oregi, X., Rodríguez-Vidal, Í., Baïri, A., 2021. Improving energy performance of historic buildings through hygrothermal assessment of the envelope. Buildings 11, 410.
Methods of test for mortar for masonry - Part 3: Determination of consistence of fresh mortar (by flow table), EN 1015-3," European Committee of Standardization, 1999.
Methods of Test for Mortar for Masonry - Part 18: Determination of Water Absorption Coefficient due to Capillary Action of Hardened Mortar, EN 1015-18, 2002. European Committee of Standardization.
Methods of Testing Cement. Part 1: Determination of Strength, EN 196-1, 2018. European Committee for Standardization.
Milone, D., Peri, G., Pitruzzella, S., Rizzo, G., 2015. Are the best available technologies the only viable for energy interventions in historical buildings? Energy Build. 95, 39–46.
Miranda, J., Valença, J., Costa, H., Júlio, E., 2022. Methodology for the restoration of heritage built in exposed concrete. The case study of 'Piscina das Marés', Portugal. Constr. Build. Mater. 328, 127040.
Mitran, R.-A., Ioniță, S., Lincu, D., Berger, D., Matei, C., 2021. A review of composite phase change materials based on porous silica nanomaterials for latent heat storage applications. Molecules 26 (1), 241.
Navarro-Blasco, Í., Perez-Nicolas, M., Fernández, J., Duran, A., Sirera, R., Álvarez, J., 2014. Assessment of the interaction of polycarboxylate superplasticizers in hydrated lime pastes modified with nanosilica or metakaolin as pozzolanic reactives. Constr. Build. Mater. 73, 1–12.
Odgaard, T., Bjarløv, S., Rode, C., 2018. Interior insulation – experimental investigation of hygrothermal conditions and damage evaluation of solid masonry façades in a listed building. Build. Environ. 129, 1–14.
Pajek, L., Potočnik, J., Košir, M., 2022. The effect of a warming climate on the relevance of passive design measures for heating and cooling of European single-family detached buildings. Energy Build. 261, 111947.
Pavlíková, M., Kapicová, A., Pivák, A., Záleská, M., Lojka, M., Jankovský, O., Pavlík, Z., 2021. Zeolite lightweight repair renders: effect of binder type on properties and salt crystallization resistance. Materials 14 (13), 3760.
Peng, H., Zhang, D., Ling, X., Li, Y., Wang, Y., Yu, Q., She, X., Li, Y., Ding, Y., 2018. n-Alkanes phase change materials and their microencapsulation for thermal energy storage: a critical review. Energy Fuels 32 (7), 7262–7293.
Posani, M., Veiga, R., Peixoto de Freitas, V., 2021. Retrofitting historic walls: feasibility of thermal insulation and suitability of thermal mortars. Heritage 4 (3), 2009–2022.
Redondo, G.P., Franco, G., Georgiou, A., Ioannou, I., Lubelli, B., Musso, S.F., Naldini, S., Nunes, C., Vecchiattini, R., 2021. State of conservation of concrete heritage buildings: a European screening. Infrastructures 6 (8), 109.
Rodríguez, C.R., Filho, F.F., Figueiredo, S.C., Schlangen, E., Šavija, B., 2020. Fundamental investigation on the frost resistance of mortar with microencapsulated phase change materials. Cement Concr. Compos. 113, 103705.
Rubio-Aguinaga, A., Fernández, J., Navarro-Blasco, Í., Álvarez, J., 2024a. Air lime renders with microencapsulated phase change materials: assessment of microstructural and thermal properties. Constr. Build. Mater. 452, 138862.
Rubio-Aguinaga, A., Fernández, J., Navarro-Blasco, Í., Álvarez, J., 2024b. Study on the interaction of polymeric chemical additives with phase change materials in air lime renders. Polymers 16 (8), 1121.
Rubio-Aguinaga, A., Kyriakou, L., Fernández, J., Navarro-Blasco, Í., Álvarez, J., 2025b. Microstructural analysis of bio-based PCM-enhanced lime mortars: durability and energy efficiency for sustainable buildings. Constr. Build. Mater. 481, 141569.
Rubio-Aguinaga, A., Kyriakou, L., Fernández, J., Navarro-Blasco, Í., Pavia, S., Álvarez, J., 2025a. Sustainability of PCM-lime mortars for heritage retrofitting: carbon footprint and impact on energy demand across climates. Case Stud. Constr. Mater. 23, e05294.
Sala, E., Zanotti, C., Passoni, C., Marini, A., 2016. Lightweight natural lime composites for rehabilitation of historical heritage. Constr. Build. Mater. 125, 81–93.
Santos, A., Veiga, M., Silva, A.S., 2023. Characterization and assessment of performance of innovative lime mortars for conservation of building heritage: paimogo's fort, a case study. Appl. Sci. 13 (8), 4679.
Sarcinella, A., Barroso De Aguiar, J., Lettieri, M., Cunha, S., Frigione, M., 2020. Thermal performance of mortars based on different binders and containing a novel sustainable Phase Change Material (PCM). Materials 13 (9), 2055.
Shadnia, R., Zhang, L., Li, P., 2015. Experimental study of geopolymer mortar with incorporated PCM. Constr. Build. Mater. 84, 95–102.
Shi, J., Tan, J., Lui, B., Liu, Y., Xu, H., Wang, Z., Xiong, T., Shi, J., 2020. Thermal and mechanical properties of thermal energy storage lightweight aggregate mortar incorporated with phase change material. J. Energy Storage 32, 101719.
Silva, B.A., Guerreiro, E., Duarte, A.P., 2025. Comparative study of lime-based mortars for conservation and restoration interventions. Constr. Build. Mater. 499, 143956.
Sinka, M., Bajare, D., Jakovics, A., Ratnieks, J., Gendelis, S., Tihana, J., 2019. Experimental testing of phase change materials in a warm-summer humid continental climate. Energy Build. 195, 205–215.
Specification for Mortar for Masonry - Part 1: Rendering and Plastering Mortar, 2018. European Committee of Standardization.
Standard Test Method for Density of Hydraulic Cement, 2023. ASTM International.
Theodoridou, M., Kyriakou, L., Ioannou, I., 2016. PCM-enhanced lime plasters for vernacular and contemporary architecture. Energy Proc. 97, 539–545.
Theodoridou, M., Kyriakou, L., Ioannou, I., 2026. Optimized lime-based renders with Phase Changing Materials (PCMs) for energy-efficient and climate resilient traditional and contemporary structures. Energy Build., 117069
Tian, C., Ahmad, N.A., Abd Rased, A.N., Xiong, Y., Li, W., 2025. Enhancing thermal comfort and energy efficiency in residential buildings using phase change materials in dual-seasonal climate zones. Results Eng. 27, 106273.
Tripathi, B.M., Shukla, S.K., 2024. A comprehensive review of the thermal performance in energy efficient building envelope incorporated with phase change materials. J. Energy Storage 79, 110128.
Ventolà, L., Vendrell, M., Giraldez, P., 2013. Newly-designed traditional lime mortar with a phase change material as an additive. Constr. Build. Mater. 47, 1210–1216.
Yeon, J.H., Kim, K.-K., 2018. Potential applications of phase change materials to mitigate freeze-thaw deteriorations in concrete pavement. Constr. Build. Mater. 177, 202–209.
Young, B.A., Falzone, G., Wei, Z., Sant, G., Pilon, L., 2018. Reduced-scale experiments to evaluate performance of composite building envelopes containing phase change materials. Constr. Build. Mater. 162, 584–595.
Zheng, Z., Shen, W., Li, S., Li, C., Yin, P., Guan, M., Ha, J., 2025. Mechanical properties and freeze-thaw durability of concrete modified with microencapsulated phase change materials. Sci. Rep. 15, 29423.